PRELIMINARY PARALLAXES OF 40 L AND T DWARFS FROM THE US NAVAL OBSERVATORY INFRARED ASTROMETRY PROGRAM

F. J. VRBA, A. A. HENDEN,[1] C. B. LUGINBUHL, H. H. GUETTER, J. A. MUNN, AND B. CANZIAN

US Naval Observatory, Flagstaff Station, P.O. Box 1149, Flagstaff, AZ 86002; fjv@nofs.navy.mil, aah@nofs.navy.mil, cbl@nofs.navy.mil, guetter@nofs.navy.mil, jam@nofs.navy.mil, blaise@nofs.navy.mil

A. J. BURGASSER[2]

Division of Astronomy and Astrophysics, UCLA, 405 Hilgard Avenue, Los Angeles, CA 90095-1562; adam@astro.ucla.edu

J. DAVY KIRKPATRICK

Infrared Processing and Analysis Center, MS 100-22, California Institute of Technology, 770 South Wilson Avenue, Pasadena, CA 91125; davy@ipac.caltech.edu

X. FAN

Steward Observatory, University of Arizona, 933 North Cherry Avenue, Tucson, AZ 85721; fan@as.arizona.edu

T. R. GEBALLE

Gemini Observatory, 670 North A'ohoku Place, Hilo, HI 96720; tgeballe@gemini.edu

D. A. GOLIMOWSKI

Department of Physics and Astronomy, Johns Hopkins University, 3400 North Charles Street, Baltimore, MD 21218; dag@pha.jhu.edu

G. R. KNAPP

Department of Astrophysical Sciences, Princeton University, Princeton, NJ 08544; gk@astro.princeton.edu

S. K. LEGGETT

UK Infrared Telescope, Joint Astronomy Centre, 660 North A'ohoku Place, Hilo, HI 96720; s.leggett@jach.hawaii.edu

D. P. SCHNEIDER

Department of Astronomy and Astrophysics, 525 Davey Laboratory, Pennsylvania State University, University Park, PA 16802; dps@astro.psu.edu

AND

J. BRINKMANN

Apache Point Observatory, P.O. Box 59, Sunspot, NM 88349; jb@apo.nmsu.edu

ABSTRACT

We present preliminary trigonometric parallaxes and proper motions for 22 L dwarfs and 18 T dwarfs measured using the ASTROCAM infrared imager on the US Naval Observatory (USNO) 1.55 m Strand Astrometric Reflector. The results presented here are based on observations obtained between 2000 September and 2002 November; about half of the objects have an observational time baseline of $\Delta t = 1.3$ yr and half $\Delta t = 2.0$ yr. Despite these short time baselines, the astrometric quality is sufficient to produce significant new results, especially for the nearer T dwarfs. Seven objects are in common with the USNO optical CCD parallax program for quality control and seven in common with the European Southern Observatory 3.5 m New Technology Telescope parallax program. We compare astrometric quality with both of these programs. Relative to absolute parallax corrections are made by employing Two Micron All Sky Survey and/or Sloan Digital Sky Survey photometry for reference-frame stars. We combine USNO infrared and optical parallaxes with the best available California Institute of Technology (CIT) system photometry to determine M_J, M_H, and M_K values for 37 L dwarfs between spectral types L0 and L8 and 19 T dwarfs between spectral types T0.5 and T8 and present selected absolute magnitude versus spectral type and color diagrams, based on these results. Luminosities and temperatures are estimated for these objects. Of special interest are the distances of several objects that are at or near the L-T dwarf boundary so that this important transition can be better understood. The previously reported early to mid T dwarf luminosity excess is clearly confirmed and found to be present at J, H, and K. The large number of objects that populate this luminosity-excess region indicate that it cannot be due entirely to selection effects. The T dwarf sequence is extended to $M_J \approx 16.9$ by 2MASS J041519−0935, which, at $d = 5.74$ pc, is found to be the least luminous [$\log (L/L_\odot) = -5.58$] and coldest ($T_{\rm eff} \approx 760$ K) brown dwarf known. Combining results from this paper with earlier USNO CCD results we find that, in contrast to the L dwarfs, there are no examples of low-velocity ($V_{\rm tan} < 20$ km s^{-1}) T dwarfs. This is consistent with the T dwarfs in this study being generally older than the L dwarfs. We briefly discuss future directions for the USNO infrared astrometry program.

Key words: astrometry — color-magnitude diagrams — stars: distances — stars: late-type — stars: low-mass, brown dwarfs

---

[1] Universities Space Research Association.
[2] Hubble Fellow.

1. INTRODUCTION

After the era of photographic proper motion surveys (e.g., Luyten 1979) revealed late M stars close to the limit of stellar hydrogen burning, a long, and largely frustrating, pursuit of substellar objects was begun by many researchers. These efforts were motivated by the overarching desire to understand the Galactic mass and luminosity distributions of putative objects that would bridge the gap between the lowest mass stars and giant planets and by the fact that no theory of star formation could be considered complete without accounting for the mass function of such objects. Becklin & Zuckerman (1988) identified GD 165B as the first object clearly cooler than an M dwarf, followed several years later by the discovery of the first "methane dwarf," Gl 229B (Nakajima et al. 1995; Oppenheimer et al. 1995); an object cold enough that its spectrum shows strong methane absorption, similar to the giant gas planets. These "brown dwarfs" became the prototypes for L (Kirkpatrick et al. 1999; Martín et al. 1999) and T dwarfs (Burgasser et al. 2002a; Geballe et al. 2002), respectively.

It was not, however, until deep, large-scale optical surveys (the Sloan Digital Sky Survey [SDSS];[3] York et al. 2000; Abazajian et al. 2003) and near-infrared surveys (the Two Micron All Sky Survey [2MASS;[4] Skrutskie et al. 1997] and the Deep Near Infrared Survey of the Southern Sky [DENIS;[5] Delfosse et al. 1997; Epchtein 1997]) of the sky were undertaken that significant numbers of field brown dwarfs were revealed. L dwarfs from these surveys have been identified by many authors (Delfosse et al. 1997; Kirkpatrick et al. 1999, 2000; Fan et al. 2000; Hawley et al. 2002; Geballe et al. 2002; Schneider et al. 2002), as have T dwarfs (Burgasser et al. 1999; Strauss et al. 1999; Tsvetanov et al. 2000; Leggett et al. 2000; Burgasser et al. 2002a; Geballe et al. 2002; Burgasser et al. 2003a; Knapp et al. 2004), among many others. Comprehensive summaries of field brown dwarf discoveries are maintained at the Web sites maintained by Kirkpatrick for L dwarfs,[6] by Burgasser for T dwarfs,[7] and by Leggett for both L and T dwarfs.[8] Currently, there are more than 250 L dwarfs and 58 T dwarfs known.

Unlike stars, brown dwarfs are not massive enough to sustain continuous hydrogen fusion in their cores, but cool continually from their birth. Somewhere between early and mid-L is the crossover between hydrogen-burning stars and brown dwarfs. Unfortunately, other than objects in clusters (Basri 2000), it is difficult to establish ages for brown dwarfs, since their spectra do not always exhibit a known direct indicator of age such as from Li destruction. This results in degeneracies among mass, age, and luminosity. However, for all but the youngest objects, brown dwarf radii are largely independent of mass and age, and all are similar to the radius of Jupiter (Chabrier & Baraffe 2000). Thus, luminosity scales well with $T_{\rm eff}^4$, with L dwarfs having surface temperatures in the range 2200–1400 K, while T dwarfs have temperatures down to about 700 K (e.g., Kirkpatrick et al. 2000; Leggett et al. 2001; Leggett et al. 2002; Dahn et al. 2002; Burgasser at al. 2002a; Golimowski et al. 2004; this paper). Obviously, an accurate measurement of the distances to these objects is required to determine their luminosities and temperatures, along with understanding many other issues, such as their cooling curves and surface flux redistribution due to atmospheric dust formation.

In earlier work, US Naval Observatory (USNO) optical CCD parallaxes and proper motions were presented for eight late M dwarfs, 17 L dwarfs, and three T dwarfs (Dahn et al. 2002, hereafter D02). Most recently, Tinney, Burgasser, & Kirkpatrick (2003, hereafter TBK03) presented near-infrared parallaxes and proper motions of nine T dwarfs. In this paper, we present preliminary trigonometric parallaxes and proper motions, obtained at near-infrared wavelengths, of 22 L dwarfs and 18 T dwarfs plus four additional L or T dwarf companion objects in binaries. We feel compelled to present preliminary parallaxes and proper motions now because of the intense interest by the community in distance determinations to these objects, rather than waiting approximately another 2 yr of observational time baseline before final results would be available for most of the objects. Final results will be presented in later papers.

2. DEVELOPMENT OF NEAR-INFRARED ASTROMETRIC CAPABILITIES AT USNO

In the mid 1990s, USNO anticipated a need to have the capability of carrying out high-accuracy relative astrometry at near-infrared wavelengths. This was based on the possibility that results from the upcoming 2MASS, DENIS, and SDSS sky surveys might reveal large numbers of brown dwarfs and other cool and dust-embedded objects that would be better detected in the near-infrared than at visible wavelengths. This need was also consistent with the USNO mission of testing the astrometric capabilities of new technology array detectors and extending this investigation to longer wavelengths. While the near-infrared offered the prospects of better detection for cool objects with smaller differential color refraction and somewhat better seeing than in the optical, the effects on astrometry of telescope and variable sky background radiation, along with the additional infrared camera optics needed to apodize emissive telescope parts and the performance of infrared array detectors themselves, were not known. Astrometric testing was carried out between 1995 and 1999 at USNO using a Rockwell HgCdTe 256^2 (NICMOS2) array in a camera not optimized for astrometric work. Repeated observations were obtained during this time frame of stars in the clusters M67 and NGC 7790 with J, H, and K magnitudes between about 11 and 14. For observations with seeing $\leq 1''.5$, we found mean errors of unit weight for a single observation of 7, 10, and 11 mas for J, H, and K, respectively (Vrba et al. 2000). These results, while not as good as those obtained with CCDs (Dahn 1997), encouraged us to pursue instrumentation specifically designed for carrying out a routine astrometric program in the near-infrared.

A major problem encountered was that, at reasonable pixelization, 256^2 format devices offer fields of view that typically are not large enough to present an adequate reference frame. Thus, in 1993, USNO joined with its partner institution the National Optical Astronomical Observatory to fund the development of the ALADDIN 1024^2 InSb array detector (Fowler et al. 1996) at the Santa Barbara Research Corporation (now Raytheon Vision Systems). This partnership led to the successful development of ALADDIN arrays, which are now used throughout astronomy. In 1996, USNO and the Naval Research Laboratory jointly began designing an ALADDIN-based camera. Mauna Kea Infrared (MKI) was contracted to build this camera, known as ASTROCAM, which was

[3] See http://www.sdss.org.
[4] See http://www.ipac.caltech.edu/2mass.
[5] See http://cdsweb.u-strasbg.fr/denis.html.
[6] See http://spider.ipac.caltech.edu/staff/davy/ARCHIVE.
[7] See http://www.astro.ucla.edu/adam/homepage/research/tdwarf.
[8] See http://www.jach.hawaii.edu/skl/LTdata.html.

delivered to the USNO, Flagstaff Station, in 1999 August. For 20 months, ASTROCAM was operated with an engineering-grade detector, during which time we optimized operation of the camera and developed an operational plan for making brown dwarf astrometric observations. In 2000 April, a science-grade ALADDIN array was installed, and in 2000 September the full parallax and proper-motion program for brown dwarfs was initiated.

3. INSTRUMENTATION

ALADDIN array detectors (Fowler et al. 1996) have 27 μm pixels with essentially 100% fill factor and approximately 85% quantum efficiency between 0.9 and 5 μm. The array is designed with quadrant architecture and eight outputs per quadrant. The particular array that we employ in ASTROCAM has dark current of about 0.7 e^- s^{-1} at its operating temperature of 30 K and has a full well capacity of about 2.1×10^5 e^- at its operating -0.8 V bias level. With double correlated sampling, we obtain a read noise of about 30 e^- rms. Except for an avoided region near one edge, which was overthinned during fabrication and which covers about 3% of the area of the array, our device has pixel operability of greater than 99.99%.

ASTROCAM was delivered by MKI as a turnkey system including Digital Signal Processor DSP-based electronics and a graphical user interface and is used exclusively at the 1.55 m Kaj Strand Astrometric Reflector at the USNO, Flagstaff Station. Since one of ASTROCAM's missions is astrometric measurements, its structure was designed to minimize flexure. The heart of ASTROCAM is an all-reflective Offner 1:1 re-imaging system, which eliminates refractive optics except for the entrance window and filters, which are tilted at 5° to avoid production of ghost images. Thus the ALADDIN 27 μm pixels are at the natural telescope scale providing 0$\farcs$3654 pixelization and a field of view of about 6$\farcm$2 × 6$\farcm$2. Determination of the pixel scale was accomplished by observation of stellar clusters with well-determined astrometric positions. Pupil plane apodization of the telescope structure is accomplished via a mask deposited on the secondary mirror of the Offner reimager for the outside edge of the optics and a light trap cone to mask the telescope primary mirror central hole. The telescope secondary support struts are not apodized. The system is telecentric so that misfocus does not change the focal plane scale. The Offner system provides image spot sizes of less than 0.5 pixel even at the very corners of the array. Field distortion has been measured, by observation with ASTROCAM of astrometric calibration fields made with the Flagstaff Astrometric Scanning Transit Telescope (FASTT; Stone 1997), at less than 100 mas rms over the entire field, a number that is dominated by the FASTT astrometric accuracy. Two 10-position concentric filter wheels currently house seven broadband filters (Z, J, H, K, K', K-long, L') and nine narrowband astrophysical filters, plus a cold blank position. An extensive description of the ASTROCAM system is given by Fischer et al. (2003).

4. OBSERVATIONAL PROCEDURES

ASTROCAM is scheduled on the 1.55 m telescope from 11 to 14 nights each lunation during bright time. Approximately 75% of the scheduled time is used for observations on the infrared parallax and proper-motion program. Observations are carried out under seeing conditions up to 2$\farcs$5 FWHM, although, in practice, the exposure times get prohibitively long for some of the fields at 2$\farcs$5. Despite the fact that differential

color refraction (DCR) in the near-infrared is smaller than in the optical, we continue the CCD parallax program practice of only obtaining observations as objects cross the meridian. Because of this, we do not apply DCR corrections, although we may consider testing DCR corrections on some fields in the future.

Prior to starting our parallax program, we carried out test astrometric observations of several L and T dwarfs in the J, H, and K bands. Best results were obtained when L dwarfs were observed in H band and T dwarfs in J band, reflecting the highest signal-to-background noise ratio (S/N) for each kind of object. With the exception of two objects, noted below, we continue to observe T dwarfs in J band and L dwarfs in H band.

Exposure times are set by the desire to not saturate either the parallax object or reference-frame stars and range from 30 to 60 s, with the number of co-adds under nominal conditions ranging from 8 to 20, with approximately twice as many co-adds employed under the most marginal conditions. A typical integration time for a single telescope dithered position is 10 minutes in nominal conditions and 20 minutes for a faint field under poor conditions. These relatively long exposure times are necessary because the 1.55 m telescope has a small effective aperture due to its large secondary mirror. Since our total integration times for a given field can range from 20 to 60 minutes, all exposures are guided by an optical wavelength leaky guider. These relatively long exposure times are another reason why we do not obtain observations off the meridian, since the large DCR between the infrared imaging and optical guiding would be transferred to the infrared images.

Three dithered integrations are obtained for each observation. The dither offset between positions is 10$''$, with the dither pattern being north-south or east-west around the nominal position, depending on the distribution of the reference-frame stars. The nominal registration of each field is repeated to within a few pixels for each visitation of a field. We have chosen to stay with a minimum number of dithers based on our tests, which show that astrometric quality is not affected by pixel sampling even under the best seeing conditions we experience.

5. DATA PROCESSING AND ASTROMETRIC REDUCTION PROCEDURES

The data processing procedures are again a product of extensive testing of astrometric solutions with ASTROCAM during the period before the astrometric program began. The first step is that all frames used in processing, program, and flats, are linearized via a process similar to that described by Luginbuhl et al. (1998) for our earlier NICMOS2 device. Linearization improves the astrometric centroiding somewhat since it has the effect of slightly sharpening the image profile. After linearization all program frames are flat fielded. We use dome flats, which are composed of the difference frames of three dome flat screen illuminated and unilluminated sets. The difference frames are median-combined into a single flat-field frame for each filter employed. After flat fielding, the program frames are passed through a min/max value filter to construct a sky frame that is subtracted from each program frame.

Astrometry is performed on individual program frames, processed as described above, not on combined frames. Centroiding for the parallax target object and the reference-frame stars is accomplished via a two-dimensional Gaussian fit technique (Monet & Dahn 1983), which is also employed in the USNO optical CCD parallax program. The astrometric

solutions are determined via the techniques and software developed by D. G. Monet (Monet & Dahn 1983; Monet et al. 1992), which are again borrowed from the USNO optical program and modified for use in our infrared program to accommodate such factors as highly varying net backgrounds. As in the optical CCD program, we use only linear frame constants and allow frame scale and rotation to be free parameters. (In fact, we do solve for second- and third-order frame constants, but discard them as they are always trivial compared with their solution errors.) All reference stars used in the reference frame are given unit weighting.

6. WHAT IS MEANT BY "PRELIMINARY" ASTROMETRIC RESULTS?

There are several considerations that make the parallax and proper-motion results we present in this paper "preliminary" rather than final. While our observing program is continuing, due to the intense interest in brown dwarfs, we decided to use the observations in hand at the end of the 2002 November observing run to provide these preliminary astrometric results. Since observations were initiated in 2000 September, this meant that about half of the fields had been observed for a time baseline Δt of about 2.0 yr and about half for only 1.3 yr. Normally, we would allow a minimum 3 yr of observing to allow uniform coverage of the observable part of the parallactic ellipse, add time baseline to the proper-motion determinations, add to $\sqrt{n}$ statistics, and have a complete separation of parallax from proper-motion solutions.

Second, the parallax results we report here are only for the X (right ascension) solutions and do not include the Y (declination) solutions weighted by error. The astrometric errors we find for ASTROCAM are nearly as good in Y as they are in X (see § 11) and, of course, we have to employ both X and Y astrometry to derive proper motions. However, since the parallactic ellipse is a circle at the ecliptic pole and a line in the ecliptic plane, the Y parallax determination is always worse than the X determination except at the pole. Thus, Y parallax solutions with the short Δt as of 2002 November range from having internal S/N of 10 down to 1. Rather than publishing combined values for only those cases for which the Y determination helped the solution, we feel that it is more straightforward to publish the X-determined solutions at this time. When we publish final parallaxes, we will present fully combined X and Y solutions.

Third, we are not employing the best astrometric reference frames for our preliminary solutions. The reference frames we use here are based on those stars for which we have adequate optical and/or infrared photometry to determine a photometric parallax for use in determining the correction from relative to absolute parallax for each frame (see § 9 on absolute parallax corrections). Naturally, it is best to use as many stars as possible that are well distributed over the field to produce the most robust reference frame. For most fields, we have at least some stars that serve as otherwise excellent reference-frame stars, but for which we do not have adequate photometry, and thus they cannot be employed in our solution. Although it is the case that the corrections from relative to absolute parallax are typically dwarfed by the parallaxes of these objects, it is not formally correct to include reference stars for which we have no photometric parallaxes. It is one of our goals to obtain the necessary photometry in order to employ the best possible reference frames when we publish final parallaxes.

Finally, we have not solved for nor culled any stars in the reference frames that might have measurable proper motions.

This should have no effect on the parallax solutions, since parallax and proper-motion solutions are largely orthogonal and should have minimal effect on proper motions since there are numerous reference-frame stars used in each solution. This will mostly have the effect of increasing the apparent errors of our global frame solutions (see § 11 on astrometric quality).

Despite these shortcuts, the preliminary parallax and proper motions we present here agree with the previously published results for objects in common and produce relatively tight spectral type–absolute magnitude diagrams. We are confident that our results are significant to within the errors we publish. Nonetheless, we caution that these are preliminary results.

7. OBJECTS ON THE PROGRAM

In Table 1, we list the full designations of the 40 L and T dwarfs or multiple systems with which we began our initial near-infrared parallax program in 2000 September and for all of which we are reporting preliminary results. Hereafter, we use an abbreviated designation for each object. There are, in fact, 44 L and T dwarfs for which we have parallactic information since four of the objects (2MASS J085035+1057AB, 2MASS J122554−2739AB, 2MASS J172811+3948AB, and 2MASS J210115+1756AB) are known doubles, which we discuss later. The 40 initial objects were selected primarily to complement those that were already being observed on the USNO optical parallax program. Specifically, this meant an emphasis on T dwarfs and a selection of late L dwarfs, all of which were difficult to observe with optical CCDs. Twenty-two of the objects are L dwarfs, and 18 are T dwarfs. Seven objects (2MASS J055919−1404, 2MASS J082519+2115, 2MASS J085035+1057, SDSS J125453−0122, SDSS J162414+0029, 2MASS J163229+1904, and 2MASS J222443−0158) were chosen to be observed in parallel with the USNO optical program in order to provide independent determinations of parallaxes and proper motions and to serve as quality control for both programs. Some of the objects had already been published at the time we began our program, while others were provided to us by members of the 2MASS and SDSS teams as part of the USNO collaboration in these surveys. Twenty-two of the objects are from the 2MASS survey, while 18 are from the SDSS survey. Column (2) of Table 1 provides the adopted spectral type from the literature (see § 13).

Column (3) of Table 1 gives the broadband filter (J or H) in which the astrometry is done for these objects. Note that, contrary to our methodology described above (that we observe L dwarfs in the H filter and T dwarfs in the J filter), two of the objects (SDSS J015141+1244 and SDSS J020742+0000) are T dwarfs being observed in the H filter. This is due to the fact that at the time we started observations they were thought to be L dwarfs, but were later determined to be T dwarfs. Rather than starting a new series of observations, we decided to simply continue the observations in the H filter, although at the expense of optimal detection S/N.

Columns (4) and (5) give the number of nights on which each object has been observed and the timespan over which the observations have been taken, respectively. The 18 objects between right ascension 10^h and 18^h have been observed for an average of 21.2 nights and an average timespan of 1.34 yr, while those between right ascension 18^h and 10^h have been observed for an average of 26.7 nights but with a significantly longer average elapsed time of 2.03 yr. This is an artifact of our decision to use data taken through

TABLE 1
Observations and Reference Stars

Star (1)	Spectral Type (2)	Filter (3)	No. of Nights (4)	Δt (yr) (5)	Mean Epoch (6)	No. Reference Stars (7)	Rel.→Abs. (8)
2MASS J00303013−1450333............	L7	H	31	2.18	2001.800	10	IR
SDSS J003259.37+141037.1.............	L8	H	23	2.02	2002.159	14	H, S, IR
SDSS J010752.42+004156.3.............	L5.5	H	34	1.87	2002.308	6	H, S
SDSS J015141.69+124429.6.............	T1 ± 1	H	26	2.03	2002.216	12	H, S, IR
SDSS J020742.83+000056.2.............	T4.5	H	20	1.93	2002.218	9	H, S, IR
2MASS J02431371−2453298............	T6	J	26	2.20	2001.774	5	IR
2MASS J03284265+2302051............	L8	H	22	2.19	2001.745	9	IR
2MASS J04151954−0935066............	T8/T9	J	20	2.12	2002.035	5	IR
SDSS J042348.57−041403.5.............	L7.5/T0	H	21	2.02	2002.248	9	IR
SDSS J053952.00−005901.9.............	L5	H	22	2.02	2001.970	10	IR
2MASS J05591914−1404488............	T5	J	27	2.10	2001.875	14	IR
2MASS J07271824+1710012............	T7	J	28	2.02	2001.906	17	IR
2MASS J08251968+2115521............	L7.5	H	16	1.88	2001.926	14	IR
SDSS J083008.12+482847.4.............	L8	H	11	1.87	2001.969	11	H, S
SDSS J083717.21−000018.0.............	T0.5	J	10	1.78	2002.016	12	H, S, IR
2MASS J08503593+1057156AB......	L6+L/T	H	13	1.86	2001.791	8	IR
2MASS J09373487+2931409............	T6p	J	14	1.87	2001.984	6	IR
2MASS J09510549+3558021............	L6	H	15	1.28	2001.725	9	IR
SDSS J102109.69−030420.1.............	T3	J	15	1.31	2001.743	8	H, S, IR
2MASS J10475385+2124234............	T6.5	J	22	1.32	2001.739	7	IR
2MASS J12171110−0311131............	T7.5	J	18	1.30	2001.848	4	H, S, IR
2MASS J12255432−2739466AB	T6:+T8:	J	14	1.30	2001.919	12	IR
2MASS J12373919+6526148............	T6.5e	J	13	1.38	2001.802	6	H, S, IR
SDSS J125453.90−012247.4.............	T2	J	15	1.29	2001.905	13	H, S, IR
SDSS 132629.81−003831.4.............	L8?	H	17	1.38	2001.829	10	H, S, IR
SDSS J134646.43−003150.4.............	T6	J	22	1.39	2001.901	9	H, S, IR
SDSS J143517.20−004612.9.............	L0	H	24	1.39	2001.925	4	H, S
SDSS J143535.72−004347.0.............	L3	H	24	1.39	2001.923	6	H, S
SDSS J144600.60+002452.0.............	L5	H	25	1.36	2001.916	5	H, S
2MASS J15232263+3014562............	L8	H	32	1.36	2001.888	10	IR
SDSS J162414.36+002915.8.............	T6	J	24	1.37	2001.920	6	H, S
2MASS J16322911+1904407............	L8	H	22	1.38	2001.852	8	IR
2MASS J17114573+2232044............	L6.5	H	26	1.36	2001.983	16	H, S, IR
2MASS J17281150+3948593AB......	L7+L/T	H	24	1.38	2001.978	11	IR
SDSS J175032.96+175903.9.............	T3.5	J	29	1.24	2001.077	26	H, S, IR
2MASS J18410861+3117279............	L4pec	H	39	2.03	2002.048	19	IR
2MASS J21011544+1756586AB......	L7.5+L8?	H	48	2.18	2002.055	17	IR
2MASS J22244381−0158521...........	L4.5	H	50	2.20	2001.969	6	IR
SDSS J225529.09−003433.4.............	L0:	H	44	2.10	2002.101	13	H, S
2MASS J23565477−1553111...........	T6	J	43	2.20	2001.939	10	IR

the observing run of 2002 November as the preliminary database.

Column (6) gives the mean epoch of the observations for each object. Column (7) gives the number of reference-frame stars employed in the solution, while column (8) gives a code describing how the conversion from relative to absolute parallax was determined for each reference frame, as explained in § 9.

8. REFERENCE FRAME SELECTION

Registration of the parallax fields was determined by taking several test exposures and choosing a registration that left as many potential reference-frame stars in the field of view of the array, but left the parallax target object as close to the field center as possible. Once observations were begun, a few processed frames with the best seeing available were inspected to rule out any extended objects or double stars as potential reference-frame members. When adequate time had elapsed so that running astrometric solutions was practical,

solutions were started using the full potential reference frame, and stars identified as degrading the solution were discarded. The stars removed were typically significantly fainter than the mean reference-frame brightness or very near the edge of the array. Finally, stars that did not have adequate photometry from which a photometric parallax could be determined were removed, as discussed above. Since we consider the reference frames used for these preliminary results to be provisional, we will defer, until such time as we publish final parallax results, a full discussion of the reference frames employed, including identification and magnitude range.

9. RELATIVE TO ABSOLUTE PARALLAX CORRECTIONS

Although the target objects of this program are nearby, we nevertheless determined corrections from relative to absolute parallaxes via photometric parallaxes for the reference-frame stars using optical photometry from SDSS and/or infrared

photometry from 2MASS. In all cases, photometric parallaxes were derived assuming that reference-frame stars are main-sequence dwarfs. We used dereddened (using the extinction maps of Schlegel, Finkbeiner, & Davis 1998) SDSS colors for those reference-frame stars with SDSS photometry (2MASS J121711−0311, 2MASS J123739+6526, 2MASS J171145+2232, and all SDSS fields except SDSS J042348−0414 and SDSS J053952−0059, which lie outside the official SDSS coverage). Since the average reference-frame star distance is ≈630 pc (1.59 mas, see below), we applied the full thin-disk reddening of the Schlegel et al. (1998) maps. For red stars ($i-z > 0.5$), we used the M_i versus $i-z$ calibration of Hawley et al. (2002). For blue stars ($i-z < 0.5$), we used the M_R versus $R-I$ calibration of Siegel et al. (2002). The $r-i$ colors were transformed to $R-I$ colors using the transformations given by Smith et al. (2002). The r magnitudes were transformed to R magnitudes using the equation $R = r - 0.21(r-i) - 0.17$ (D. Tucker 2003, private communication). Only those blue stars in the color range $0.3 < R-I < 1.5$ had photometric parallaxes derived. This is slightly bluer than the range adopted by Siegel et al. (who used a blue cutoff of 0.4); the calibration still fits the dwarf sequence to $R-I = 0.3$, although confusion with turnoff stars becomes greater.

For fields without SDSS photometry, but with 2MASS photometry, we transformed the 2MASS $J-H$ and $H-K$ colors to California Institute of Technology (CIT) colors (Elias et al. 1982) using the transformations of Carpenter (2001). The transformed colors were used to estimate spectral types from the spectral type versus infrared color calibration (transformed to the CIT system) of Bessell & Brett (1988). Absolute V magnitudes as a function of spectral type were taken from Schmidt-Kaler (1982) and converted to M_J and M_K via the Bessell & Brett (1988) calibrations. Distances were determined by averaging $(m - M)_J$ and $(m - M)_K$. Since extinction in the J and K bands is only a small fraction of that in the optical, reddening in the infrared was ignored. For the fields for which both SDSS and 2MASS colors were available, the average distance was taken. Column (7) of Table 1 gives the codes H, S, or IR indicating whether the Hawley et al. (2002), Siegel et al. (2002), and/or infrared calibrations were employed.

Since we give each reference-frame star equal weight in the astrometric solution, the distances in milliarcseconds for each star are simply averaged and a standard deviation of the mean calculated for each reference frame. The reference-frame distances in milliarcseconds are added to the relative parallax astrometric solutions in milliarcseconds and the errors of the reference-frame distance corrections are added in quadrature to the relative parallax astrometric errors. The average correction to absolute parallax is 1.59 mas, with average uncertainty 0.31 mas, and scatter 0.46 mas (s.d.). The average correction for the 16 fields observed in the J filter is 1.70 mas, while for the 24 fields observed in the H filter it is 1.52 mas.

The mean ratio of $\Delta\pi_{\mathrm{rel}\rightarrow\mathrm{abs}}/\pi_{\mathrm{abs}}$ is 0.036 ± 0.026, indicating that the mean correction adds only a few percent to the distance of these objects. The mean ratio of $\sigma(\Delta\pi_{\mathrm{rel}\rightarrow\mathrm{abs}})/\sigma(\pi_{\mathrm{rel}})$ is 0.087 ± 0.059, indicating that the error of the corrections to absolute parallax, when added in quadrature, adds almost nothing to the total parallax error. The mean ratio of $\sigma(\Delta\pi_{\mathrm{rel}\rightarrow\mathrm{abs}})/\pi_{\mathrm{abs}}$ is 0.008 ± 0.014, confirming that the error of the relative to absolute parallax correction is small compared with the parallaxes themselves for these objects.

Finally, we note that there are 76 reference-frame stars distributed among 12 fields for which $\Delta\pi_{\mathrm{rel}\rightarrow\mathrm{abs}}$ was based on both SDSS optical and 2MASS infrared photometry. The mean difference between these (SDSS−2MASS) is $+0.10 \pm 0.08$ (s.d.m.) mas. Thus, there is no significant systematic difference in the reference-frame distances estimated from SDSS and 2MASS.

10. ASTROMETRIC RESULTS

Table 2 presents our preliminary proper-motion and parallax results. The first column gives an abbreviated object name. The second column gives the spectral type that we adopt (see § 13). The third column gives the parallax (π) solution relative to the reference frame employed along with the standard mean error. The fourth column gives the absolute parallax, which is corrected for the estimated distances to the reference-frame stars as described in § 9, along with its standard mean error. The error for the absolute parallaxes contains, in quadrature, the sum of the error of the relative parallax determination with the error of the absolute parallax correction. Comparing the relative and absolute parallaxes and their errors demonstrates the small effect of the distance of the reference frame for these relatively nearby objects. The fifth column gives the relative proper motion (μ) in milliarcseconds per year with respect to the reference frame along with the formal uncertainty. The sixth column gives the position angle of the proper motion (in the sense east of north), along with its uncertainty. Using SDSS astrometric stars in the field for SDSS J053952−0059 for 41 frames spaced over 2 yr, we found the mean rotation of the field as $-0°044 \pm 0°063$. Thus, the natural rotation of ASTROCAM, when pointed at the meridian and $\delta \approx 0°$, is indistinguishable from the celestial system, so we have made no rotation correction to the natural position angle. Finally, in the last column, we give the tangential velocity with respect to the Sun by combining the absolute parallax and relative proper-motion results.

11. ASTROMETRIC QUALITY

For the group of 18 objects with an average 21.2 nights and average $\Delta t = 1.34$ yr, the mean parallax error is 4.86 mas and the mean proper motion error is 8.23 mas yr^{-1}. For the group of 22 objects with an average 26.7 nights and average $\Delta t = 2.03$ yr, the mean parallax error is 3.86 mas and the mean proper motion error is 5.20 mas yr^{-1}. Thus, the proper-motion errors scale with $(\Delta t)^{-1}$ as might be expected if the observations are uniformly distributed. The parallax errors reduce somewhat faster than if proportional to nights^{-1}. The most likely reason for this is that the objects with the smaller time baseline do not as yet have observations well distributed over parallax factor. Certainly, the objects with only 1.34 yr of observations must be viewed with some degree of caution in this regard, although the spectral type versus absolute magnitude figures discussed below would indicate that there are no gross errors for any object. While we have chosen to not present the Y (declination) parallax results at this time, we note that the slope $\pi(Y)/\pi(X)$ is 0.99 ± 0.05 and that the $\pi(X)$ and $\pi(Y)$ results for all objects agree to within their error bars.

As Monet et al. (1992) have pointed out, the mean error for a single observation of unit weight (m.e.1) for an ensemble of stars on frames taken over a period of time is a useful measure of astrometric accuracy. They report a range of 3−5 mas as characteristic of fields observed in the USNO

TABLE 2
Astrometric Results

Star	Spectral Type	π_{rel} (mas)	π_{abs} (mas)	μ_{rel} (mas yr^{-1})	P.A. (deg)	V_{tan} (km s^{-1})
2MASS J003030−1450...................	L7	35.39 ± 4.49	37.42 ± 4.50	246.6 ± 3.6	96.56 ± 0.42	31.2 ± 3.8
SDSS J003259+1410......................	L8	28.82 ± 5.16	30.14 ± 5.16	275.8 ± 6.9	81.83 ± 0.72	43.4 ± 7.7
SDSS J010752+0041......................	L5.5	61.98 ± 4.48	64.13 ± 4.51	634.5 ± 7.1	81.71 ± 0.32	46.9 ± 3.3
SDSS J015141+1244......................	T1 ± 1	45.26 ± 3.36	46.73 ± 3.37	742.7 ± 4.2	92.84 ± 0.16	75.3 ± 5.5
SDSS J020742+0000......................	T4.5	33.15 ± 9.86	34.85 ± 9.87	156.3 ± 11.4	96.29 ± 2.09	21.3 ± 6.7
2MASS J024313−2453...................	T6	90.23 ± 3.50	93.62 ± 3.63	354.8 ± 4.1	234.20 ± 0.33	18.0 ± 0.7
2MASS J032842+2302...................	L8	31.06 ± 4.19	33.13 ± 4.20	61.0 ± 4.9	168.08 ± 2.30	8.7 ± 1.3
2MASS J041519−0935...................	T8/T9	172.87 ± 2.75	174.34 ± 2.76	2255.3 ± 3.2	76.48 ± 0.04	61.4 ± 1.0
SDSS J042348−0414......................	L7.5/T0	64.50 ± 1.69	65.93 ± 1.70	333.1 ± 2.8	284.23 ± 0.24	24.0 ± 0.6
SDSS J053952−0059	L5	74.43 ± 2.16	76.12 ± 2.17	356.1 ± 3.5	27.49 ± 0.28	22.2 ± 0.7
2MASS J055919−1404...................	T5	93.84 ± 1.43	95.53 ± 1.44	655.2 ± 2.8	121.10 ± 0.12	32.5 ± 0.5
2MASS J072718+1710...................	T7	109.01 ± 2.34	110.14 ± 2.34	1296.5 ± 4.5	126.25 ± 0.10	55.8 ± 1.2
2MASS J082519+2115...................	L7.5	94.20 ± 1.83	95.64 ± 1.84	584.5 ± 4.0	239.45 ± 0.20	29.0 ± 0.6
SDSS J083008+4828......................	L8	74.93 ± 3.42	76.42 ± 3.43	1267.0 ± 6.5	232.58 ± 0.15	78.6 ± 3.6
SDSS J083717−0000......................	T0.5	32.44 ± 13.45	33.70 ± 13.45	173.0 ± 16.7	185.05 ± 2.76	24.3 ± 11.8
2MASS J085035+1057AB	L6+L/T	24.76 ± 4.21	26.22 ± 4.21	147.2 ± 6.2	261.93 ± 1.20	26.6 ± 4.5
2MASS J093734+2931...................	T6p	161.47 ± 3.87	162.84 ± 3.88	1622.0 ± 7.1	143.14 ± 0.13	47.2 ± 1.1
2MASS J095105+3558...................	L6	14.88 ± 7.40	16.09 ± 7.40	189.4 ± 10.6	211.83 ± 1.60	55.8 ± 32.7
SDSS J102109−0304	T3	39.13 ± 11.00	40.78 ± 11.00	179.4 ± 15.2	246.24 ± 2.42	20.9 ± 6.3
2MASS J104753+2124...................	T6.5	92.82 ± 3.76	94.73 ± 3.81	1728.4 ± 7.7	254.08 ± 0.13	86.5 ± 3.5
2MASS J121711−0311	T7.5	108.63 ± 5.87	110.36 ± 5.88	1061.8 ± 10.2	274.95 ± 0.27	45.6 ± 2.5
2MASS J122554−2739AB	T6:+T8:	72.76 ± 3.46	74.20 ± 3.47	736.9 ± 6.8	147.80 ± 0.26	47.1 ± 2.3
2MASS J123739+6526...................	T6.5e	93.82 ± 4.75	96.07 ± 4.78	1131.4 ± 8.9	242.33 ± 0.23	55.8 ± 2.8
SDSS J125453−0122	T2	74.51 ± 2.87	75.71 ± 2.88	483.2 ± 6.1	284.45 ± 0.36	30.3 ± 1.2
SDSS J132629−0038	L8?	49.01 ± 6.33	49.98 ± 6.33	250.6 ± 8.9	244.63 ± 1.02	23.8 ± 3.2
SDSS J134646−0031	T6	71.13 ± 5.01	72.74 ± 5.02	491.5 ± 10.0	254.31 ± 0.58	32.0 ± 2.3
SDSS J143517−0046	L0	8.42 ± 5.10	9.85 ± 5.18	24.7 ± 9.2	64.99 ± 10.65	11.9 ± 9.7
SDSS J143535−0043	L3	15.28 ± 5.76	16.07 ± 5.76	107.5 ± 8.8	168.27 ± 2.34	31.7 ± 13.3
SDSS J144600+0024......................	L5	43.04 ± 3.21	45.46 ± 3.25	191.2 ± 7.0	110.06 ± 1.05	19.9 ± 1.6
2MASS J152322+3014...................	L8	55.77 ± 3.27	57.30 ± 3.27	221.4 ± 5.9	139.77 ± 0.76	18.3 ± 1.2
SDSS J162414+0029......................	T6	84.94 ± 3.82	86.85 ± 3.85	374.0 ± 6.0	269.65 ± 0.46	20.4 ± 1.0
2MASS J163229+1904...................	L8	62.17 ± 3.31	63.58 ± 3.32	301.7 ± 5.1	101.37 ± 0.48	22.5 ± 1.2
2MASS J171145+2232...................	L6.5	31.48 ± 4.80	33.11 ± 4.81	31.2 ± 7.5	98.35 ± 6.88	4.5 ± 1.2
2MASS J172811+3948AB	L7+L/T	40.33 ± 3.26	41.49 ± 3.26	45.0 ± 6.4	125.17 ± 4.07	5.1 ± 0.9
SDSS J175033+1759......................	T3.5	35.07 ± 4.53	36.24 ± 4.53	204.3 ± 7.8	60.80 ± 1.09	26.7 ± 3.5
2MASS J184108+3117...................	L4 pec	22.12 ± 1.88	23.57 ± 1.89	72.6 ± 3.7	55.00 ± 1.46	14.6 ± 1.4
2MASS J210115+1756AB	L7.5+L8?	29.04 ± 3.42	30.14 ± 3.42	208.5 ± 3.7	136.33 ± 0.51	32.8 ± 3.8
2MASS J222443−0158...................	L4.5	83.43 ± 1.46	85.01 ± 1.50	980.6 ± 2.0	151.35 ± 0.06	54.7 ± 1.0
SDSS J225529−0034	L0:	14.61 ± 2.56	16.19 ± 2.59	179.9 ± 2.6	191.61 ± 0.41	52.7 ± 8.7
2MASS J235654−1553...................	T6	66.96 ± 3.38	68.97 ± 3.42	746.2 ± 2.9	216.46 ± 0.11	51.3 ± 2.6

CCD parallax program on the 1.55 m telescope. For our preliminary data, we find mean errors and standard deviations in X and Y, respectively, of 15.5 ± 4.9 and 17.9 ± 4.9 mas (8.9 ± 2.8 and 10.3 ± 2.9 mas for dithered triplets, which are equivalent to one CCD observation). There is no significant difference between fields observed in J or H. These results improve considerably when solutions are run using only the four brightest reference-frame stars with X and Y errors, respectively, of 8.1 ± 3.4 and 10.0 ± 4.1 (4.6 ± 1.9 and 5.8 ± 2.4 for dithered triplets). There is no obvious reason why the Y errors are systematically larger than X.

There are several likely reasons why the infrared astrometric accuracies are somewhat worse than for CCD results at the same telescope. The first is that we have thus far not solved for proper motions for any of the reference-frame stars. While largely orthogonal to the parallax solution, allowing for proper motions in the reference frame should significantly reduce m.e.1. Second, we have not made corrections for DCR, although, since our observations are in the infrared and are

constrained to the meridian, we believe this has little effect. A third issue is the quality of some frames we have had to employ to produce a preliminary set of results. Figure 1 shows the histogram of seeing at the beginning of each set of observations employed in this paper. Although the median image size is 1″.33 (FWHM), we have had to employ many frames with much worse seeing. Experience from the USNO CCD program has shown that astrometric quality is not significantly degraded when exposure times are increased by (image size)^2 so as to maintain a central image density. However, due to the small effective aperture of our telescope, our exposure times are typically 30 minutes for three dithers even in the best seeing. Thus, we can afford to only double exposure times in worse seeing. While the poorer seeing frames, at this point, help the parallax solution, they clearly hurt the m.e.1 statistics. As we accumulate more data over a longer time baseline the poorer seeing observations will be retired.

It is instructive to compare our infrared astrometric accuracy with that found by TBK03. Using the European Southern
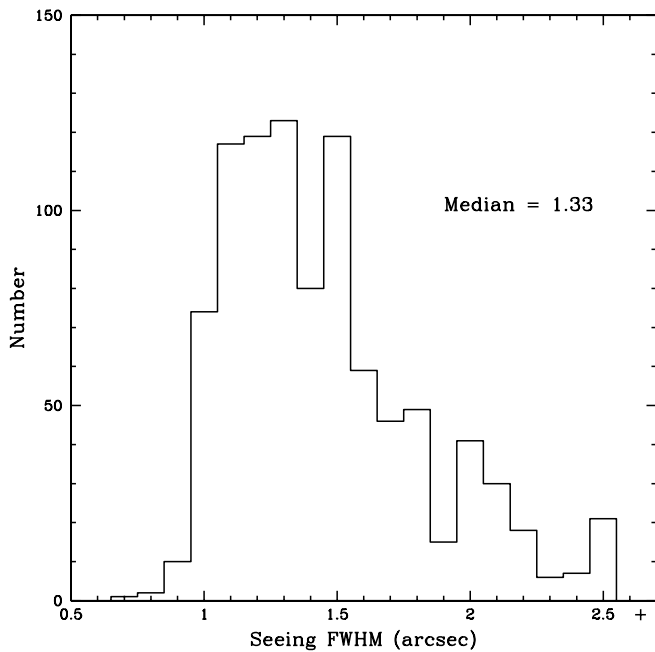
Fig. 1.—Histogram of the seeing (in the J and H bands) at the 1.55 m telescope using ASTROCAM at the beginning of each set of observations employed in this paper. The bar at $2\rlap{.}''5+$ represents those observations at $2\rlap{.}''5$ and slightly larger used in the solutions. The median seeing is $1\rlap{.}''33$.

Observatory (ESO) 3.5 m New Technology Telescope (NTT) with $0\rlap{.}''815$ FWHM median seeing, they find an m.e.1 of 12.1 mas (0.042 pixels) for each 2 minute individual frame. From above, we find an XY-averaged m.e.1 of 16.7 mas (0.046 pixels) for each typical 10 minute individual frame using a 1.55 m telescope with $1\rlap{.}''33$ FWHM median seeing.

12. COMPARISON OF π AND μ TO PREVIOUS RESULTS

12.1. *USNO CCD Program*

Table 3 compares the results for the seven objects in common between the USNO infrared and optical CCD programs (D02). Column (1) gives the abbreviated object names, the second column whether CCD, IR, or difference values, and the third column the range of time (ΔT) over which the observations were observed. The fourth column gives the derived absolute parallaxes, errors, and differences. While it is true that the CCD and IR parallaxes are derived using different reference frames, correction to absolute parallax should give consistent results. The fifth and sixth columns give the relative proper motions and position angles of proper motion and their errors, respectively, along with differences.

There are two objects that have marginally different parallaxes. One is 2MASS J085035+1057, which is a binary of $0\rlap{.}''16$ separation (Reid et al. 2001, discussed in § 15.4) and for which the IR and CCD programs also derive marginally different proper-motion position angles. Using our IR parallax, $0\rlap{.}''16$ semimajor axis, and the maximum mass of the system (Reid et al. 2001), we estimate a minimum orbital period of the system of ≥ 51 yr. Given the short ΔT values of both programs it is unlikely that orbital motion of the system could lead to major errors in the parallax or proper-motion determinations. In addition, our analysis in § 15.4 indicates similar spectral types for the two binary members, so that the photometric barycenters should not be strongly affected in either the optical or infrared. More observations in both programs will be needed of this system to ensure that the derived parallax is without systematic errors.

The second object with marginally different parallaxes is SDSS J125453−0122. There is no indication that this object is in a binary system. We see in § 12.2 that the USNO IR parallax is nearly identical with that measured by TBK03, so we favor

TABLE 3
Comparison of USNO Infrared and Optical Results

Star (1)	Program (2)	Δt (yr) (3)	π_{abs} (mas) (4)	μ_{rel} (mas yr^{-1}) (5)	P.A. (deg) (6)
2MASS J055919−1404...............	CCD[a]	2.1	97.7 ± 1.3	661.2 ± 1.2	121.6 ± 0.1
	IR	2.10	95.53 ± 1.44	655.2 ± 2.8	121.10 ± 0.12
	CCD-IR	...	+2.2 ± 1.9	+6.0 ± 3.0	−0.5 ± 0.2
2MASS J082519+2115...............	CCD[a]	2.0	93.8 ± 1.0	585.6 ± 1.4	240.5 ± 0.2
	IR	1.88	95.64 ± 1.84	584.5 ± 4.0	239.45 ± 0.20
	CCD-IR	...	−1.8 ± 2.1	+1.1 ± 4.2	+1.0 ± 0.3
2MASS J085035+1057AB	CCD[a]	3.3	39.1 ± 3.5	144.7 ± 2.0	267.0 ± 0.9
	IR	1.86	26.22 ± 4.21	147.2 ± 6.2	261.93 ± 1.20
	CCD-IR	...	+12.9 ± 5.5	−2.5 ± 6.5	+5.1 ± 1.5
SDSS J125453−0122..................	CCD[a]	1.2	84.9 ± 1.9	496.1 ± 1.8	285.2 ± 0.4
	IR	1.29	75.71 ± 2.88	483.2 ± 6.1	284.45 ± 0.36
	CCD-IR	...	+9.2 ± 3.4	+12.9 ± 6.4	+0.7 ± 0.6
SDSS J162414+0029..................	CCD[a]	2.2	91.5 ± 2.3	383.2 ± 1.9	269.6 ± 0.5
	IR	1.37	86.85 ± 3.85	374.0 ± 6.0	269.65 ± 0.46
	CCD-IR	...	+4.6 ± 4.5	+9.2 ± 6.3	−0.0 ± 0.7
2MASS J163229+1904...............	CCD[a]	3.2	65.6 ± 2.1	298.0 ± 0.9	100.4 ± 0.2
	IR	1.38	63.58 ± 3.32	301.7 ± 5.1	101.37 ± 0.48
	CCD-IR	...	+2.0 ± 3.9	−3.7 ± 5.2	−1.0 ± 0.5
2MASS J222443−0158...............	CCD[a]	2.3	88.1 ± 1.1	983.8 ± 0.7	152.3 ± 0.1
	IR	2.20	85.01 ± 1.50	980.6 ± 2.0	151.35 ± 0.06
	CCD-IR	...	+3.1 ± 1.9	+3.8 ± 2.1	+0.9 ± 0.2
Weighted Mean Diff.	...	...	+2.6 ± 1.4	+3.9 ± 1.5	+0.3 ± 0.1

[a] From D02.

TABLE 4
COMPARISON OF INFRARED ASTROMETRIC RESULTS

Star (1)	Program (2)	Δt (yr) (3)	π_{rel} (mas) (4)	μ_{rel} (mas yr^{-1}) (5)	P.A. (deg) (6)
SDSS J102109−0304	USNO	1.31	39.13 ± 11.00	179.4 ± 15.2	246.24 ± 2.42
	ESO[a]	1.7	34.4 ± 4.6	183.2 ± 3.4	248.8 ± 1.0
	U-E		+4.7 ± 11.9	−3.8 ± 15.6	−2.6 ± 2.6
2MASS J104753+2124	USNO	1.32	92.82 ± 3.76	1728.4 ± 7.7	254.08 ± 0.13
	ESO[a]	1.9	110.8 ± 6.6	1698.9 ± 2.5	256.4 ± 0.1
	U-E		−18.0 ± 7.6	+29.5 ± 8.1	−2.3 ± 0.2
2MASS J121711−0311	USNO	1.30	108.63 ± 5.87	1061.8 ± 10.2	274.95 ± 0.27
	ESO[a]	1.9	90.8 ± 2.2	1057.1 ± 1.7	274.1 ± 0.1
	U-E		+17.8 ± 6.3	+4.7 ± 10.3	+0.9 ± 0.3
2MASS J122554−2739AB	USNO	1.30	72.76 ± 3.46	736.9 ± 6.8	147.80 ± 0.26
	ESO[a]	1.9	75.1 ± 2.5	736.8 ± 2.9	148.5 ± 0.1
	U-E		−2.3 ± 4.3	+0.1 ± 7.4	−0.7 ± 0.3
SDSS J125453−0122	USNO	1.29	74.51 ± 2.87	483.2 ± 6.1	284.45 ± 0.36
	ESO[a]	1.7	73.2 ± 1.9	491.0 ± 2.5	284.7 ± 0.1
	U-E		+1.3 ± 3.4	−7.8 ± 6.6	−0.3 ± 0.4
SDSS J134646−0031	USNO	1.39	71.13 ± 5.01	491.5 ± 10.0	254.31 ± 0.58
	ESO[a]	1.7	68.3 ± 2.3	516.0 ± 3.3	257.2 ± 0.2
	U-E		+2.8 ± 5.5	−24.5 ± 10.5	−2.9 ± 0.6
SDSS J162414+0029	USNO	1.37	84.94 ± 3.82	374.0 ± 6.0	269.65 ± 0.46
	ESO[a]	1.9	90.9 ± 1.2	373.0 ± 1.6	268.6 ± 0.3
	U-E		−6.0 ± 4.0	+1.0 ± 6.2	1.1 ± 0.5
Weighted Mean Diff. (USNO-ESO)			−0.4 ± 3.1	+1.0 ± 5.7	−1.0 ± 0.6

[a] From TBK03.

the USNO IR parallax over the USNO CCD parallax. (We note that the USNO optical measurement is based on only $\Delta T = 1.2$ yr, so the discrepancy may just be due to a small ΔT.)

The last line of Table 3 gives the weighted mean differences in parallax, proper motion, and proper-motion position angle between the USNO IR and CCD determinations. There is no strong evidence for any systematic differences in these quantities determined between the two programs.

12.2. *ESO 3.5 m NTT Infrared Program*

Earlier (§ 11) we discussed the differences in astrometric quality between the USNO infrared program and the infrared program that has been carried out at the ESO 3.5 m NTT (TBK03). Table 4 compares the parallax and proper-motion results for the seven objects in common between the infrared programs at USNO and at ESO. Column (1) gives the abbreviated object names, the second column whether USNO, ESO, or difference values, and the third column the range of time (Δt) over which the observations were obtained. Since TBK03 did not apply corrections to absolute parallax, in the fourth column we compare relative parallaxes and their errors. The fifth and sixth columns give the relative proper motions and position angles of proper motion and their errors, respectively.

One of the objects, 2MASS J122554−2739AB, is in a binary system (see § 15.6); however, there is no significant difference between the parallaxes, proper motions, and position angles determined by both programs. The only marginally significant differences are for both the parallax and proper motion of 2MASS J104753+2124 and the parallax of 2MASS J121711−0311. It is not possible to understand which determination is better at this time, although we note that, for this object and all others in Table 4, the USNO observations are all in the shorter time baseline group of $\Delta t \approx 1.3$ yr.

The last line of Table 4 gives the weighted mean differences in parallax, proper motion, and proper-motion position angle between the USNO and ESO determinations. There is no evidence for any systematic differences in these quantities determined between the two programs.

13. ADOPTED SPECTRAL TYPES AND INFRARED PHOTOMETRY

We compile here the spectral types and infrared photometry, primarily from the literature, to be used in the ensuing discussion. In Table 5, we present a small amount of USNO infrared photometry relevant to the objects discussed in this paper. The data are an addendum to the USNO photometry obtained with IRCAM presented by D02, which gives details of the observations and reductions. These data are essentially on the CIT photometric system, since they were obtained by normalization to the Elias et al. (1982)–based standards of Guetter et al. (2003). The exceptions to this are the data for SDSSJ020742+0000, for which we used 2MASS All-Sky Point Source Catalog (PSC) photometry of stars within the field of view of ASTROCAM, converted those to CIT system values via the transformations of Carpenter (2001), and used instrumental ASTROCAM *JHK* magnitudes to obtain *JHK* photometry for this object. This process was adopted because 2MASS did not obtain photometry for this faint object, and there are no published empirical transformations between photometry on other systems and the CIT system for T dwarfs. Stephens & Leggett (2004) have published synthetic transformations, but in this paper we chose to employ empirical transformations only (see below).

In Table 6, we present adopted spectral types and combined *JHK* photometry on the CIT system (Elias et al. 1982) for the 40 objects presented in this paper. Column (1) gives the abbreviated object name, column (2) the adopted spectral type,

Star	Spectral Type	$K \pm \sigma(K)$	$J{-}H \pm \sigma(J{-}H)$	$H{-}K \pm \sigma(H{-}K)$
SDSS J020742+0000[a]............	T4.5	16.52 ± 0.03	-0.12 ± 0.04	0.24 ± 0.03
SDSS J053952−0059.............	L5	12.49 ± 0.04	0.89 ± 0.04	0.55 ± 0.05
2MASS J093734+2931...........	T6p	15.55 ± 0.15	-0.12 ± 0.05	-0.85 ± 0.15
2MASS J095105+3558...........	L6	15.10 ± 0.12	1.04 ± 0.13	0.77 ± 0.16
2MASS J104753+2124...........	T6.5	16.10 ± 0.10	-0.12 ± 0.16	-0.20 ± 0.16
SDSS J134646−0031	T6	15.76 ± 0.23	-0.07 ± 0.04	0.12 ± 0.16
SDSS J162414+0029..............	T6	15.53 ± 0.12	-0.08 ± 0.03	-0.04 ± 0.12
2MASS J172811+3948AB	L7+L/T	13.96 ± 0.11	1.06 ± 0.07	0.60 ± 0.10
2MASS J210115+1756AB	L7.5+L8?	16.90 ± 0.10	. . .	. . .

[a] Based on relative photometry of 2MASS stars in the ASTROCAM field of view.

Star (1)	Spectral Type (2)	Spectral Reference (3)	$K \pm \sigma(K)$ (4)	$(J{-}H) \pm \sigma(J{-}H)$ (5)	$(J{-}K) \pm \sigma(J{-}K)$ (6)	Photometric Reference (7)
2MASS J 003030−1450	L7	1	14.51 ± 0.10	0.97 ± 0.15	1.71 ± 0.15	A
SDSS J003259+1410...................	L8	2	14.99 ± 0.05	0.99 ± 0.07	1.55 ± 0.09	A, B
SDSS J010752+0041...................	L5.5	2	13.67 ± 0.07	1.26 ± 0.05	2.05 ± 0.05	A, B
SDSS J015141+1244...................	T1 ± 1	2	15.21 ± 0.19	0.94 ± 0.17	1.32 ± 0.23	A
SDSS J020742+0000...................	T4.5	2	16.52 ± 0.03	-0.12 ± 0.04	0.24 ± 0.03	C
2MASS J024313−2453...............	T6	3	15.24 ± 0.17	0.27 ± 0.12	0.17 ± 0.18	A
2MASS J032842+2302...............	L8	1	14.88 ± 0.05	0.95 ± 0.07	1.45 ± 0.10	A, B
2MASS J041519−0935...............	T8/T9	3, 4	15.45 ± 0.20	0.19 ± 0.13	0.26 ± 0.21	A
SDSS J042348−0414...................	L7.5/T0	2, 5, 6	12.95 ± 0.03	0.94 ± 0.06	1.42 ± 0.08	A, B
SDSS J053952−0059...................	L5	7	12.50 ± 0.04	0.89 ± 0.02	1.42 ± 0.03	A, C, D
2MASS J055919−1404...............	T5	8	13.60 ± 0.05	0.15 ± 0.05	0.25 ± 0.06	A
2MASS J072718+1710...............	T7	3	15.58 ± 0.19	-0.10 ± 0.18	0.05 ± 0.20	A
2MASS J082519+2115...............	L7.5	1	13.02 ± 0.05	1.22 ± 0.06	1.95 ± 0.04	A, B, E
SDSS J083008+4828...................	L8	2, 5	13.69 ± 0.03	0.98 ± 0.09	1.60 ± 0.11	A, B
SDSS J083717−0000...................	T0.5	2, 9	16.02 ± 0.05	0.86 ± 0.07	0.97 ± 0.07	D
2MASS J085035+1057AB..........	L6 + L/T	10, 11	14.45 ± 0.04	1.13 ± 0.03	1.84 ± 0.03	A, B, E
2MASS J093734+2931...............	T6p	3	15.40 ± 0.13	-0.09 ± 0.05	-0.73 ± 0.20	A, C
2MASS J095105+3558...............	L6	1	15.13 ± 0.10	1.09 ± 0.10	1.88 ± 0.16	A, C
SDSS J102109−0304...................	T3	2, 9	15.28 ± 0.05	0.70 ± 0.05	0.78 ± 0.06	A, D
2MASS J104753+2124...............	T6.5	12	16.10 ± 0.10	-0.01 ± 0.10	-0.27 ± 0.11	A, C
2MASS J121711−0311	T7.5	12	15.70 ± 0.12	0.14 ± 0.13	0.18 ± 0.13	A, E
2MASS J122554−2739A............	T6:	12, 13, 14	15.38 ± 0.17	0.19 ± 0.09	0.19 ± 0.16	A, F
2MASS J122554−2739B............	T8:	12, 13, 14	16.73 ± 0.17	0.19 ± 0.09	0.19 ± 0.16	A, F
2MASS J123739+6526...............	T6.5e	12	16.15 ± 0.20	-0.04 ± 0.09	-0.18 ± 0.22	A, E
SDSS J125453−0122...................	T2	2, 9	13.88 ± 0.04	0.78 ± 0.03	0.96 ± 0.04	A, D
SDSS J132629−0038...................	L8?	7	14.16 ± 0.05	1.13 ± 0.08	1.92 ± 0.08	A, B
SDSS J134646−0031...................	T6	2, 15	15.78 ± 0.18	-0.07 ± 0.04	0.00 ± 0.18	A, C
SDSS J143517−0046...................	L0	16	15.35 ± 0.18	0.85 ± 0.15	1.11 ± 0.20	A
SDSS J143535−0043...................	L3	16	15.05 ± 0.14	0.81 ± 0.16	1.40 ± 0.18	A
SDSS J144600+0024...................	L5	2, 3	13.88 ± 0.08	1.14 ± 0.14	1.74 ± 0.09	A, B
2MASS J152322+3014...............	L8	1	14.31 ± 0.03	1.03 ± 0.03	1.65 ± 0.08	A, B, E
SDSS J162414+0029...................	T6	2, 17	15.53 ± 0.12	-0.07 ± 0.03	-0.12 ± 0.12	A, C
2MASS J163229+1904...............	L8	10	13.98 ± 0.03	1.18 ± 0.05	1.80 ± 0.04	A, B, E
2MASS J171145+2232...............	L6.5	1	14.75 ± 0.10	1.24 ± 0.21	2.25 ± 0.20	A
2MASS J172811+3948AB..........	L7 + L/T	1, 18	13.94 ± 0.05	1.10 ± 0.06	1.87 ± 0.15	A, C
SDSS J175033+1759...................	T3.5	2	15.50 ± 0.19	0.40 ± 0.17	0.83 ± 0.21	A
2MASS J184108+3117...............	L4 pec	1	14.24 ± 0.07	1.14 ± 0.11	1.85 ± 0.11	A
2MASS J210115+1756AB..........	L7.5 + L8?	1, 19	14.92 ± 0.12	1.09 ± 0.19	2.00 ± 0.13	A, C
2MASS J222443−0158...............	L4.5	1	12.05 ± 0.02	1.21 ± 0.04	1.95 ± 0.03	A
SDSS J225529−0034...................	L0:	20	14.33 ± 0.08	0.80 ± 0.06	1.17 ± 0.06	A, B
2MASS J235654−1553...............	T6	3	15.80 ± 0.18	0.22 ± 0.12	0.06 ± 0.19	A

REFERENCES.—(1) Kirkpatrick et al. 2000; (3) Burgasser et al. 2002a; (2) Geballe et al. 2002; (4) Knapp et al. 2004; (5) Kirkpatrick et al. 2004; (6) see § 15.2; (12) Burgasser et al. 1999; (16) Hawley et al. 2002; (20) Schneider et al. 2002; (13) Burgasser et al. 2003a; (7) Fan et al. 2000; (14) See § 15.6; (10) Kirkpatrick et al. 1999; (9) Burgasser et al. 2000; (11) See § 15.4; (9) Leggett et al. 2000; (18) See § 15.8; (19) See § 15.9; (15) Tsvetanov et al. 2000; (17) Strauss et al. 1999. (A) 2MASS Point Source Catalog; (B) Leggett et al. 2002; (E) D02; (C) Table 5, this paper; (D) Leggett et. al 2000; (F) see § 15.6.

and column (3) references for the spectral types, including the discovery reference. For L dwarfs, we have adopted spectral types based on the optical spectrum classification system of Kirkpatrick et al. (2000), supplemented by work from several other authors, while for T dwarfs we have adopted spectral types based on the infrared spectrum classification system of Burgasser et al. (2002a), supplemented by the system of Geballe et al. (2002). The three exceptions to this are for the three L dwarfs SDSS J003259+1410, SDSS J010752+0041, and SDSS J144600+0024, for which no optical classifications have been published. For SDSS J083008+4828, we use an unpublished optical classification from Kirkpatrick et al. (2004). We note that these choices leave a gap between L8 and T0, since there are, so far, no L dwarfs later than L8 classified in the Kirkpatrick et al. (2000) system. See § 15 for further discussion of spectral types for several objects of special interest.

The *JHK* photometry given in columns (4)–(6) is combined from several sources: the 2MASS All-Sky PSC[9] transformed to the CIT system by the relations of Carpenter (2001), for L dwarfs MKO photometry (Leggett et al. 2002) transformed to CIT by the relations of Hawarden et al. (2001), previously published USNO photometry (D02) that is on the CIT system (Guetter et al. 2003), UKIRT photometry for four objects (Leggett et al. 2000) transformed to the CIT system by the relations of Hawarden et al. (2001), and the small amount of new USNO CIT system photometry presented in Table 5. The listed photometric values are weighted mean values based on the published photometric errors after transformation to the CIT system. Column (7) gives references to the photometry employed.

For the purposes of this paper, we have chosen to employ published empirical transformations from the various systems to the CIT system. Stephens and Leggett (2004) have pointed out the potential dangers in using transformations based on normal stars for L and T dwarfs and have calculated synthetic transformations from various systems to the MKO system. Examination of their results show that the predicted systematic errors are only a few percent for all transformations, except for the 2MASS to CIT transformation at *K* band, which is approximately 0.05 mag for L dwarfs and ranging from 0.10 mag for early and mid T dwarfs to as large as 0.20 mag for the latest T dwarfs. However, 2MASS photometry for the late T dwarfs studied here is either unavailable or with intrinsic photometric errors at the 0.2 mag level. Thus, random errors, along with the reported 0.05–0.25 mag intrinsic variations for these objects (Enoch, Brown, & Burgasser 2003) dominate this potential source of systematic error.

14. DISCUSSION

In this section we present selected infrared absolute magnitude versus spectral type and infrared color relationships. At the risk of being accused of astronomical chauvinism, we have chosen for the remainder of this paper to discuss only USNO-derived optical and infrared parallaxes (this paper and D02). This provides a self-consistent set of parallax and proper-motion determinations using the same telescope and similar observing philosophies and reduction software, with only the detector being different. When we publish completed parallax solutions, it will then be appropriate to combine these
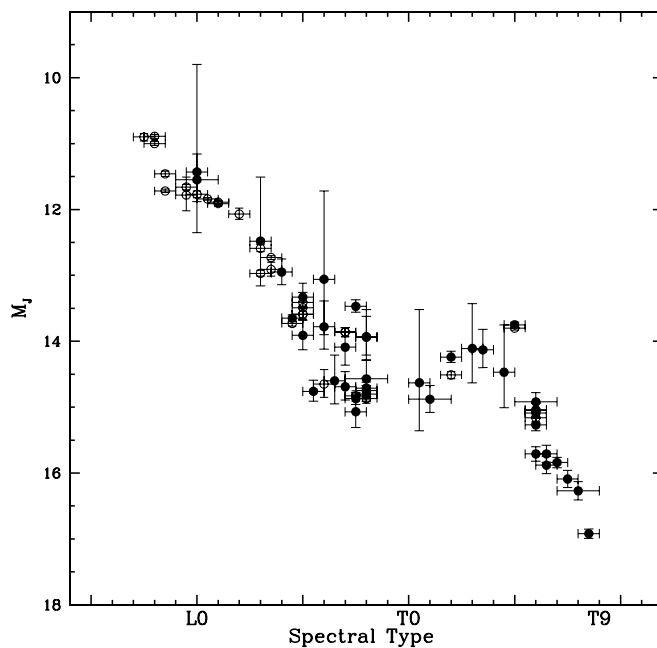
---

9 See http://www.ipac.caltech.edu/2mass.

Fig. 2.—Absolute J-band magnitude (M_J) plotted vs. spectral type. The filled data points are the results from the infrared astrometry and photometry from Table 6 of this paper; the open points are the results of optical astrometry from D02. For the seven objects in common, results are plotted for both optical and infrared parallaxes. A complete description of this figure is given in § 14.1.

results with those of other researchers. Four of the objects, 2MASS J085035+1057AB, 2MASS J122554−2739AB, 2MASS J172811+3948AB, and 2MASS J210115+1736AB are known binaries. We discuss how the separated spectral types and photometry are determined in §§ 15.4, 15.6, 15.8, and 15.9, respectively.

14.1. *Absolute Magnitude versus Spectral Type*

In Figure 2, we plot *J*-band absolute magnitude (M_J) versus spectral type. The solid data points are the results from this paper, where we have combined the infrared parallaxes with the infrared photometry and spectral classifications listed in Table 6. The photometric errors have been convolved with the parallax uncertainties to produce the vertical error bars. The horizontal errors are ±0.5 spectral type for those objects with well-determined spectral classification and ±1.0 spectral type for those with less certain classifications. The open data points are from D02, where we have used the parallaxes, infrared photometry, and spectral types published in that paper. For the seven objects in common between D02 and this paper, we plot both the CCD- and infrared-derived absolute magnitudes using the photometry of Table 6. In order to be consistent photometrically, we plot T513−46546 (D02) using 2MASS All-Sky PSC photometry transformed to CIT values by the Carpenter (2001) transformations. Several of the objects, in both the infrared and optical parallax groups, are known binaries, and we have plotted them in accordance with what is known about their binary natures. These objects are discussed individually in §§ 15 and 16 below. In Figures 3 and 4, we plot the M_H and M_K absolute magnitudes, respectively, versus spectral type with the same considerations as for Figure 2.

Our results for spectral types earlier than about L5 do not provide much new information, since we have only a few
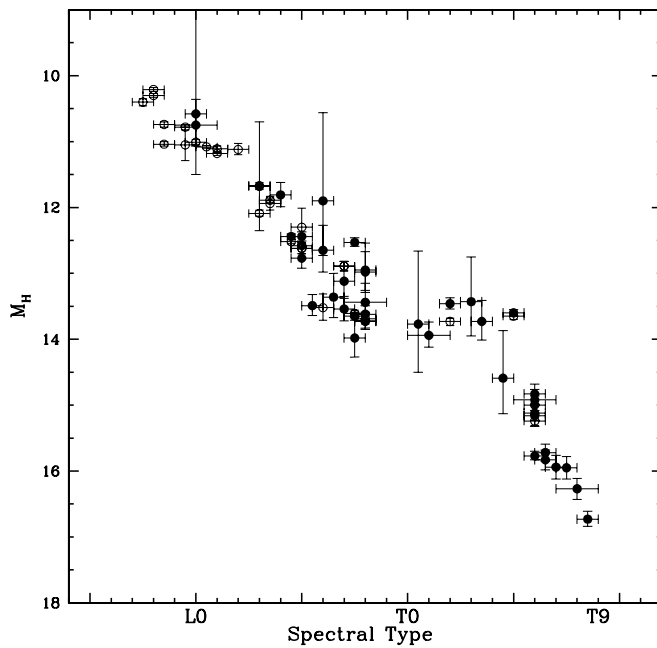
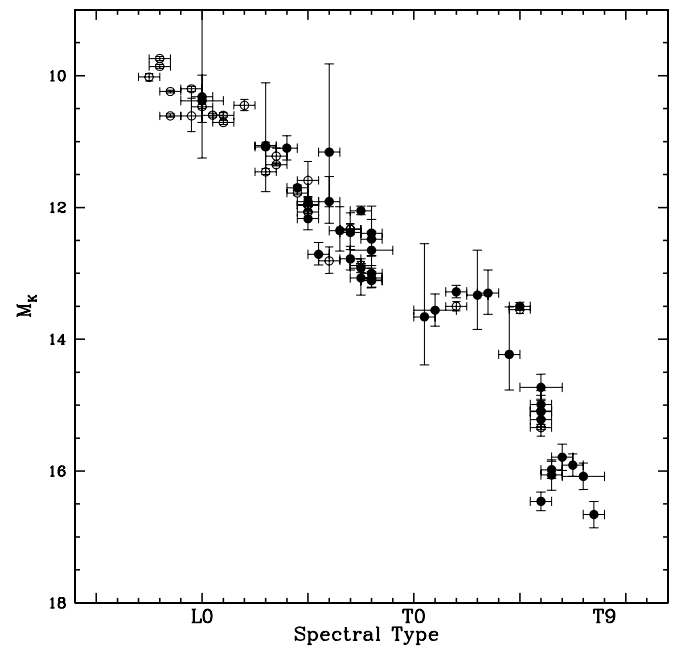Fɪɢ. 3.—Same as for Fig. 2, except for absolute *H*-band magnitude (M_H)

Fɪɢ. 4.—Same as for Fig. 2, except for absolute *K*-band magnitude (M_K)

early L dwarfs, some of which currently have large error bars. However, the results are consistent with narrow loci in all three diagrams. For objects between L5 and L8, the dispersion is clearly much greater than for earlier objects. The widths are about 1.5, 1.3, and 1.0 mag in *J*, *H*, and *K*, respectively, for the L5–L8 objects. While this could be due to an admixture of objects of different ages, masses, and gravities, we have looked, within a given spectral type, for correlations of M_J, M_H, and M_K with tangential velocities (see § 14.3) as a potential age indicator, but have found none. More likely, the additional width is due to the complicated atmospheric physics expected for late L dwarfs (Burgasser et al. 2002b; Stephens 2003), which also can explain why the spread is a function of wavelength. These models also predict significant variability due to rapid evolution or motion of cloud holes, which alone could be responsible for the apparent spread in absolute magnitude. Clearly, photometric monitoring will be necessary to fully understand the L–T transition objects.

In all three diagrams, the transition from L to T dwarfs is smooth. The excess in luminosity for T1–T5 spectral types, previously noted by D02 and TBK03, is clearly substantiated by our enhanced database. While this excess is most evident in the *J* band, it is also seen in the *H* and *K* bands. The possibility that the early T dwarf luminosity excess is caused by contamination due to binary systems (Burgasser 2001) now seems unlikely due to the sheer number of objects that participate in this hump. TBK03 point out that the amplitude of the hump, like the spread at late L, is also unlikely to be explained by an age selection effect (Tsuji & Nakajima 2003). T dwarfs between T6 and T8 once again form a rather tight locus terminating at $M_{J,H,K} \approx 16.6$.

The additional data for T dwarfs allow a somewhat clearer picture of the L–T transition region in these diagrams. While there is no self-evident reason to believe that M_J, M_H, or M_K should map linearly with spectral type (TBK03), we note that inspection of Figures 2 through 4 shows that the late T dwarfs (T6–T8) are on a rough extension of the absolute magnitude

versus spectral type relation of the early L dwarfs (L0–L5). Relative to a fiducial line drawn between the early L's and late T's, in *J* band the L–T transition objects show a luminosity deficit of about 1.5 mag at L6–L8 and a luminosity excess of about 1.5 mag at T1–T5. In *H* band, the L6–L8 deficit has shrunk to about 0.5 mag and disappears at *K* band, while in *H* and *K* bands the excess for T1–T5 objects remains at 1.0–1.5 mag.

We note that the contrast between the large spread of absolute magnitudes at late L versus the apparently narrow locus of early T absolute magnitudes may not be significant. The narrow T dwarf locus may yet prove to be an artifact of small number statistics. In addition, spectral typing may just map out an equivalent diversity of physics over a smaller range of spectral types at late L than at early T.

14.2. *Absolute Magnitude versus Infrared Colors*

In Figure 5, we plot M_J versus *J*−*H* color. The solid data points are the results from this paper, where we have combined the infrared parallaxes with the infrared photometry and spectral classifications listed in Table 6. The photometric errors have been convolved with the parallax uncertainties to produce the vertical error bars, while the horizontal errors are from Table 6. The open data points are those from D02, where we have used the parallaxes, infrared photometry, and spectral types published in that paper. We treat the seven objects in common between D02 and this paper and the binary systems as described in § 14.1. In Figure 6, we plot M_J versus *J*−*K* color, while in Figures 7 and 8 we plot M_K versus *J*−*H* and *J*−*K*, respectively.

These figures show the well-known color trends for L dwarfs ranging from *J*−*H* ≈ 0.7, *J*−*K* ≈ 1.1 for L0 ($M_J \approx 11.0$, $M_K \approx 10.0$) to *J*−*H* ≈ 1.2, *J*−*K* ≈ 2.1 for L8 ($M_J \approx 15.0$, $M_K \approx 13.5$). Late T dwarfs (T5–T8) all have roughly *J*−*H* ≈ 0, *J*−*K* ≈ 0, while early T dwarfs (T0.5–T4.5) have a wide range of colors transitioning between late L and late T colors. Several objects are now placed in the transition region between the loci of the L and T dwarfs,
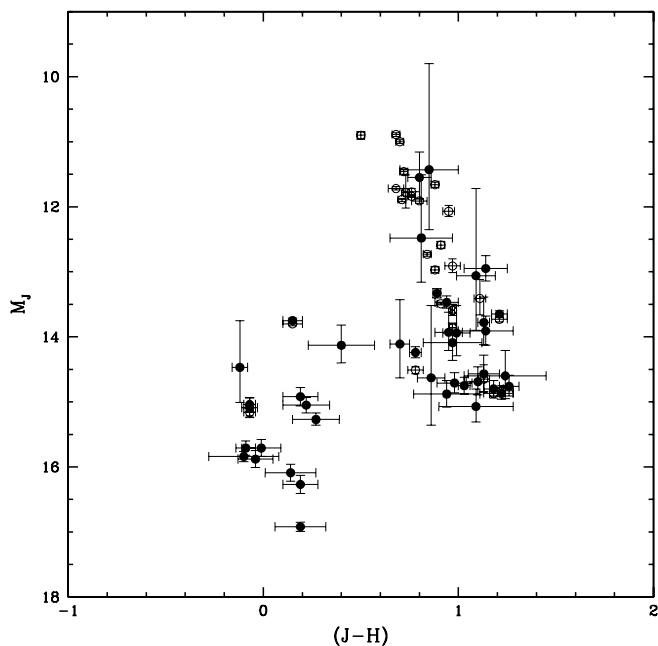
Fig. 5.—Absolute *J*-band magnitude (M_J) plotted vs. *J*−*H* color. The filled data points are the results from the infrared astrometry and photometry from Tables 2 and 6 of this paper, while the open points are the results of optical astrometry and infrared photometry from D02. For the seven objects in common, results are plotted for both optical and infrared parallaxes. A complete description of this figure is given in § 14.2.

Fig. 7.—Same as for Fig. 5, except for M_K vs. *J*−*H* color

which is best shown in the M_K versus *J*−*K* diagram (Fig. 8). Unfortunately, the locations of many of the transition objects and early T dwarfs are poorly known at this time due to uncertain distances. We will defer comparing evolutionary models with observations until we obtain final parallaxes and further USNO-CIT photometry. However, we note that the apparent brightening in M_J across the L–T transition is consistent with the predictions of the cloud hole model of Burgasser et al. (2002b), while the fact that the brightening is

an apparent trend argues against the hypothesis of Tsuji & Nakajima (2003) that it is simply an age effect.

14.3. *Kinematics*

For stars in the solar vicinity, motion with respect to the Sun is an indicator of age, since older stars will have had time to be perturbed preferentially to different orbits by interaction with the Galactic disk. Because T dwarfs are thought to be the cooler and older analogs of at least some L dwarfs, it might be expected that T dwarfs will have a larger mean velocity, with respect to the Sun, than L dwarfs. The measured tangential velocities ($V_{\rm tan}$) with respect to the Sun measured primarily for L dwarfs in D02 can be combined with those for L and
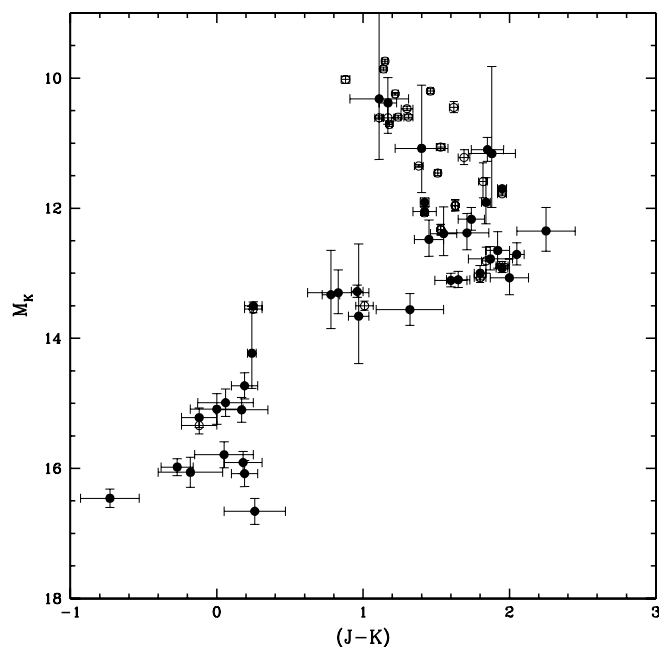

Fig. 6.—Same as for Fig. 5, except for M_J vs. *J*−*K* color

Fig. 8.—Same as for Fig. 5, except for M_K vs. *J*−*K* color
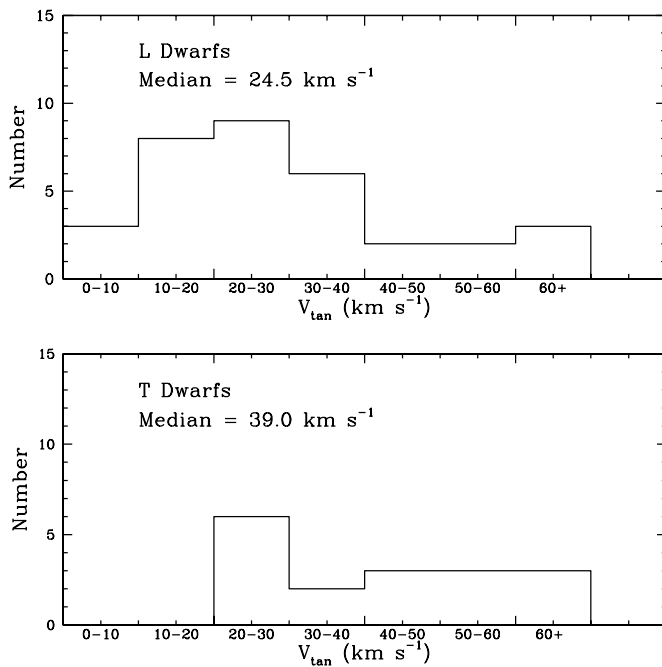
Fig. 9.—Histograms of the distributions of $V_{\rm tan}$ for L dwarfs and T dwarfs

T dwarfs in this paper (Table 2) to have sufficient objects in order to compare the velocity distributions. For the seven objects in common between the two papers, we use the weighted mean values of $V_{\rm tan}$. We remove three objects from consideration with exceptionally large $V_{\rm tan}$ uncertainties, having both $\sigma(V_{\rm tan}) > 10$ km s^{-1} and $V_{\rm tan}/\sigma(V_{\rm tan}) < 3$ (two L dwarfs, 2MASS J143535$-$0043 [31.7 $\pm$ 13.3 km s^{-1}] and 2MASS J095105+3558 [55.8 $\pm$ 32.7 km s^{-1}], and one T dwarf, SDSS J083717$-$0000 [24.3 $\pm$ 11.8 km s^{-1}]; all from this paper). This leaves 33 L dwarfs and 17 T dwarfs to make the velocity comparison. The unweighted average values of tangential velocity for L and T dwarfs, respectively, is 30.0 ± 3.6 and 43.0 ± 4.8 km s^{-1}. The median values are, for L and T dwarfs, respectively, 24.5 and 39.0 km s^{-1}. As D02 have discussed, the velocity of the L dwarfs is consistent with velocities for old disk M and dM stars.

The distributions of $V_{\rm tan}$ are shown in Figure 9 for L dwarfs in the top panel and for T dwarfs in the bottom panel. Based on the Kolmogorov-Smirnov test, the null hypothesis that the two distributions are indistinguishable can only be rejected at the 73% level. The main difference is that the T dwarfs have no examples with $V_{\rm tan} \leq 20$ km s^{-1}, whereas the L dwarfs have 11 of 33 (33%) with $V_{\rm tan} \leq 20$ km s^{-1}. While there are fewer objects in the T dwarf subset, if the distributions were the same, 5.7 T dwarfs with $V_{\rm tan} \leq 20$ km s^{-1} would be expected.

15. DISCUSSION OF INDIVIDUAL OBJECTS

There are several objects that, after our new parallax results, warrant special attention. We discuss these briefly here.

15.1. *2MASS J041519−0935*

This object is the assigned T8 standard on the Burgasser et al. (2002a) classification system, which we have adopted as the primary classification system for T dwarfs in this paper. However, in the classification system of Geballe et al. (2002), it is T9 (Knapp et al. 2004), indicating that it is likely the latest spectral type T dwarf yet found. Although it makes little

quantitative difference, we plot and fit the object as a T8.5, to recognize its extremely late spectral type. With a parallax of 174.3 ± 2.8 mas (5.74 ± 0.09 pc), it is one of the closest known brown dwarfs. Combining this distance with its 2MASS photometry gives it the lowest absolute magnitude of any T dwarf known: $M_J = 16.92 \pm 0.07$ (see § 17). We estimate a bolometric magnitude of $M_{\rm bol} = 18.70 \pm 0.26$, a luminosity of $\log(L/L_{\odot}) = -5.58 \pm 0.10$, and, hence, a temperature of $T_{\rm eff} = 760 \pm 80$ K, making it the least luminous and coldest brown dwarf yet discovered. See § 18 for our discussion of bolometric corrections and temperature estimates for T dwarfs.

15.2. *SDSS J042348−0414*

The L–T transition object SDSSJ042348$-$0414 has unusual spectral properties such that in the near-infrared Geballe et al. (2002) classify it as a T0, while in the optical Cruz et al. (2003) and Kirkpatrick et al. (2004) classify it as an L7.5. Both classifications are correct in the wavelength regions considered. It has a K-band bolometric correction that is typical of L7.5–T0 objects (Golimowski et al. 2004). At L7.5, it lies at the top of the loci for late L dwarfs in the spectral type versus absolute magnitude diagrams of Figures 2–4, about a factor of 2 brighter than the average for late L dwarfs. At T0, it lies well above the locus for early T dwarfs in these same diagrams; about a factor of 4 brighter than the average for early T dwarfs. While this could be explained by binarity (multiplicity in the case of T0), no *Hubble Space Telescope* (*HST*) observations have yet been obtained to help resolve this issue. While we have not yet carried out a formal search for perturbations, there is no evidence in the astrometric data to indicate either perturbations or difficulty in centroiding for this nearby (15.2 pc) object. From § 11, for the group of 22 objects with average $\Delta t = 2.03$ yr, the mean parallax error is 3.86 mas, and the mean proper motion error is 5.20 mas yr^{-1}. SDSS J042348$-$0414 has $\Delta t = 2.02$ yr, with mean parallax and proper-motion errors of 1.70 mas and 2.80 mas yr^{-1}, respectively. Another possibility is that this object is still very young and thus overluminous due to a radius larger than for older brown dwarfs. For the purposes of this paper, we will use the L7.5 classification, since it lies within the absolute magnitude loci of late L dwarfs, and its near-infrared colors are not inconsistent with this spectral classification. Clearly, further investigation will be needed to understand the nature of this enigmatic object.

15.3. *2MASS J055919−1404*

2MASS J055919$-$1404 has historically been considered enigmatic, since it appeared to have an absolute magnitude considerably larger than objects of similar spectral type. Although it has been suspected of being an equal mass binary (Burgasser 2001; D02), recent *HST* Wide Field Planetary Camera 2 (WFPC2) observations have failed to reveal a bright binary companion at a separation larger than 0$.''$05 (Burgasser et al. 2003a), although such a system could currently be hidden in an unfavorable orientation. Our data add considerably to the census of T1–T5 objects that populate the hump seen in the spectral type versus absolute magnitude diagrams (Figs. 2–4). These results indicate that 2MASS J055919$-$1404 lies at least much closer to the loci of other objects in this spectral range than was previously thought. It will require further luminosity determinations of other T1–T5 objects and other observations of 2MASS J055919$-$1404 itself to determine whether this object is indeed overluminous or simply the

prototype hump object lying at the peak of this local luminosity maximum.

15.4. 2MASS J085035+1057AB

2MASS J085035+1057AB was found by Reid et al. (2001) to be a binary system with a separation of $0''.16$ from *HST* WFPC2 observations. Based on optical colors from these observations they estimate a *J*-band magnitude difference of $\Delta M = 0.9$. Adopting this magnitude difference, the photometry listed in Table 6, and our parallactic distance, we find a value of $M_J = 13.78$ for the A component, which is consistent with the L6 V spectral type for the dominant component found by Kirkpatrick et al. (1999, see Fig. 2). The B component has $M_J = 14.68$, which is consistent with a late L, early T, or a T6 spectral type (again see Fig. 2). A mid to late T spectral type can probably be ruled out on the basis of the combined spectrum (Reid et al. 2001). Since late L dwarf colors range between $J-K \approx 1.6-2.0$ and early T colors cluster around $J-K \approx 1.0$, measurement of a *K* magnitude alone would likely distinguish between a late L and early T spectral type for the B component.

15.5. 2MASS J093734+2931

The second faintest T dwarf in our sample, and one of the closest (6.14 ± 0.15 pc), is 2MASS J093734+2931, which was classified as a peculiar T6 by Burgasser et al. (2002a) due to its extremely blue near-infrared color ($J-K = -0.72 \pm 0.20$; Table 6). This object is indeed peculiar, in that it is over 3 times less luminous and about 300 K cooler than the typical T6 dwarf observed (see §§ 18 and 19). Burgasser et al. (2002a, 2003b) postulate that 2MASS J093734+2931 may be a metal-poor and/or high gravity (i.e., old and massive) brown dwarf based on the enhanced collisionally induced H_2 absorption that gives it its blue near-infrared colors. These gravity/metallicity effects may be substantial enough to modify the near-infrared spectrum so that it appears to be an earlier type (hotter) brown dwarf than its true $T_{\rm eff}$. Alternatively, *K*-band bolometric corrections for this object may also be biased, due to the substantial suppression of flux at these wavelengths (Golimowski et al. 2004). However, given that this object is subluminous in all near-infrared bands as compared with other T6 dwarfs, metallicity and/or gravity differences are clearly important in these cool brown dwarfs and must be quantified before a universal spectral type/temperature relation can be derived.

15.6. 2MASS J122554−2739AB

2MASS J122554−2739 is a clearly separated double system with an angular separation of $0''.282 \pm 0''.005$ from *HST* WFPC2 observations (Burgasser et al. 2003a). Based on optical colors from these observations, they speculate that the system is composed of T6 and T8 components and estimate a *J*-band magnitude difference of $\Delta M_J = 1.35 \pm 0.08$. Adopting this magnitude difference and assuming that it also applies to the *H* and *K* band (since late T dwarf *JHK* colors scatter around 0.0), we use the available 2MASS photometry transformed to the CIT system, and apply our parallactic distance determination to produce the *JHK* absolute magnitudes listed in Table 7 (see § 17) and plotted in Figures 2–8. The infrared absolute magnitudes are consistent with T6 and T8 for components A and B, respectively.

Our parallax result increases the projected separation of the components to 3.80 ± 0.18 AU from the 3.18 AU separation based on the spectrophotometric distance (Burgasser et al. 2003a). This, in turn, increases the estimated orbital period of the system to between 31 and 53 yr, based on the effective temperatures and age range assumed by Burgasser et al. (2003a), but it does not alter their conclusion that direct orbital motion of this system could be detected over a short time range.

15.7. SDSS J143517−0046 and SDSS J143535−0043

SDSS J143517−0046 and SDSS J143535−0043 were put on the infrared parallax program partially because, at an angular separation of about $5'$, they could be a common proper motion pair. While the current parallax results do not rule out the possibility that they are at the same distance, the proper motions are nearly a factor of 4 different in magnitude and the position angles nearly orthogonal. Thus, the angular proximity of these objects appears to be fortuitous.

15.8. 2MASS J172811+3948AB

Gizis et al. (2003) found this to be a binary with $0''.13$ separation using the *HST* WFPC2 camera. They found the A component to be 0.3 mag brighter than the B component in the *I* band, but 0.3 mag fainter in the *Z* band, which they interpret as the B component being an L/T transition object. Since the $J-H$ and $J-K$ colors (Table 6) are normal for the L7 spectral classification (Kirkpatrick et al. 2000) and absolute *JHK* magnitudes are approximately equal for late L to early T, we assume that the flux is evenly split between the two components in the infrared to produce the *JHK* absolute magnitudes listed in Table 7 (see § 17) and plotted in Figures 2–8.

15.9. 2MASS J210115+1756AB

Gizis et al. (2003) found this to be a binary with $0''.232$ separation using the *HST* WFPC2 camera. They find the B component to be slightly later than the L7.5 classification of the system (Kirkpatrick et al. 2000). Since the colors and absolute *JHK* magnitudes are similar for late L dwarfs, we assume that the flux is evenly split between the two components in the infrared to produce the *JHK* absolute magnitudes listed in Table 7 (see § 17) and plotted in Figures 2–8.

16. BINARIES IN THE CCD DATA SET

There are four additional binary systems in the CCD astrometry set that we treat in a manner similar to that of D02. Two systems have components of equal near-infrared magnitudes: DENIS 020529−1159AB (Koerner et al. 1999; Leggett et al. 2001) and DENIS 122815−1547AB (Koerner et al. 1999). For these systems, we assume that the components have identical spectral types and plot the absolute magnitudes with the assumption that the flux is split evenly between the components.

In the case of 2MASS J074642+2000AB, Reid et al. (2001) estimate a *J*-band magnitude difference of $\Delta M_J = 0.47$ based on optical colors from *HST* WFPC2 observations. We use this magnitude difference to estimate the *J* magnitude for the L0.5 primary component and assume that the combined light colors apply to the primary to estimate its *H* and *K* magnitudes. While there is not enough information available to uniquely determine the nature of the B component, we note that its resultant $M_J = 12.31 \pm 0.02$ is consistent with its being about an L3 V. Since *JHK* colors of L0.5 and L3 objects are similar (Table 9), our assumption that the system *JHK* colors are

TABLE 7
INFRARED ABSOLUTE MAGNITUDES BASED ON USNO ASTROMETRY

Star	Spectral Type	Opt/IR	M_J	σ (−/+)	M_H	σ (−/+)	M_K	σ (−/+)
2MASS J034543+2540.........	L0	O	11.77	−0.05/+0.05	11.01	−0.04/+0.03	10.47	−0.04/+0.03
SDSS J143517−0046	L0	I	11.43	−1.63/+0.92	10.58	−1.63/+0.92	10.32	−1.63/+0.93
SDSS J225529−0034	L0:	I	11.55	−0.39/+0.33	10.75	−0.39/+0.32	10.38	−0.39/+0.33
2MASS J074642+2000A.......	L0.5	O	11.84	−0.02/+0.02	11.08	−0.02/+0.02	10.60	−0.03/+0.03
2MASS J143928+1929..........	L1	O	11.89	−0.02/+0.03	11.18	−0.02/+0.03	10.71	−0.03/+0.03
2MASS J165803+7027..........	L1	O	11.91	−0.04/+0.04	11.11	−0.04/+0.04	10.60	−0.04/+0.03
Kelu−1.................................	L2	O	12.07	−0.09/+0.08	11.12	−0.09/+0.08	10.45	−0.09/+0.08
DENIS J1058.7−1548..........	L3	O	12.97	−0.05/+0.04	12.09	−0.05/+0.04	11.46	−0.05/+0.04
2MASS J114634+2230A.......	L3	O	12.59	−0.06/+0.05	11.68	−0.06/+0.05	11.06	−0.05/+0.05
2MASS J143535−0043.........	L3	I	12.48	−0.97/+0.68	11.67	−0.97/+0.68	11.08	−0.97/+0.68
2MASS J003616+1821.........	L3.5	O	12.73	−0.03/+0.03	11.89	−0.03/+0.03	11.35	−0.02/+0.02
2MASS J032613+2950.........	L3.5	O	12.91	−0.11/+0.10	11.94	−0.11/+0.10	11.22	−0.12/+0.11
2MASS J184108+3117.........	L4 pec	I	12.95	−0.20/+0.19	11.81	−0.19/+0.18	11.10	−0.19/+0.18
2MASS J222443−0158.........	L4.5	I+O	13.70	−0.05/+0.05	12.49	−0.04/+0.04	11.75	−0.04/+0.04
SDSS J053952−0059	L5	I	13.33	−0.07/+0.07	12.44	−0.07/+0.07	11.91	−0.07/+0.07
DENIS J122815−1547A	L5	O	13.59	−0.09/+0.08	12.62	−0.09/+0.08	11.96	−0.09/+0.08
DENIS J122815−1547B	L5	O	13.59	−0.09/+0.08	12.62	−0.09/+0.08	11.96	−0.09/+0.08
2MASS J132855+2114.........	L5	O	13.41	−0.29/+0.25	12.30	−0.29/+0.25	11.59	−0.29/+0.25
SDSS J144600+0024.............	L5	I	13.91	−0.23/+0.22	12.77	−0.17/+0.15	12.17	−0.18/+0.17
2MASS J150747−1627.........	L5	O	13.49	−0.02/+0.02	12.58	−0.02/+0.02	12.07	−0.02/+0.02
SDSS J010752+0041	L5.5	I	14.76	−0.17/+0.15	13.49	−0.17/+0.15	12.71	−0.18/+0.16
2MASS J085035+1057A.......	L6	I+O	14.34	−0.46/+0.38	13.21	−0.45/+0.37	12.50	−0.45/+0.37
2MASS J095105+3558..........	L6	I	13.06	−1.34/+0.84	11.90	−1.34/+0.83	11.16	−1.34/+0.83
2MASS J171145+2232..........	L6.5	I	14.60	−0.39/+0.35	13.36	−0.36/+0.31	12.35	−0.36/+0.31
2MASS J003030−1450.........	L7	I	14.09	−0.30/+0.27	13.12	−0.30/+0.26	12.38	−0.30/+0.26
2MASS J172811+3948A.......	L7	I	14.69	−0.23/+0.20	13.54	−0.19/+0.18	12.78	−0.19/+0.17
DENIS J020529−1159A	L7	O	13.86	−0.07/+0.07	12.89	−0.07/+0.07	12.33	−0.08/+0.08
DENIS J020529−1159B	L7	O	13.86	−0.07/+0.07	12.89	−0.07/+0.07	12.33	−0.08/+0.08
SDSS J042348−0414	L7.5/T0	I	13.47	−0.10/+0.09	12.53	−0.07/+0.06	12.05	−0.07/+0.06
2MASS J082519+2115..........	L7.5	I+O	14.84	−0.08/+0.08	13.62	−0.04/+0.04	12.89	−0.05/+0.05
2MASS J210115+1756A.......	L7.5	I	15.07	−0.27/+0.24	13.98	−0.32/+0.29	13.07	−0.29/+0.26
SDSS J003259+1410.............	L8	I	13.94	−0.42/+0.35	12.95	−0.41/+0.34	12.39	−0.41/+0.34
2MASS J032842+2302.........	L8	I	13.93	−0.31/+0.28	12.98	−0.31/+0.28	12.48	−0.30/+0.26
SDSS J083008+4828.............	L8	I	14.71	−0.16/+0.15	13.73	−0.11/+0.10	13.11	−0.11/+0.10
SDSS J132629−0038	L8?	I	14.57	−0.29/+0.27	13.44	−0.29/+0.27	12.65	−0.29/+0.27
2MASS J152322+3014.........	L8	I	14.75	−0.13/+0.13	13.72	−0.13/+0.13	13.10	−0.13/+0.12
2MASS J163229+1904.........	L8	I+O	14.85	−0.08/+0.07	13.67	−0.08/+0.07	13.05	−0.07/+0.06
SDSS J083717−0000	T0.5	I	14.63	−1.11/+0.73	13.77	−1.11/+0.73	13.66	−1.11/+0.73
SDSS J015141+1244.............	T1 ± 1	I	14.88	−0.21/+0.20	13.94	−0.20/+0.18	13.56	−0.25/+0.24
SDSS J125453−0122	T2	I+O	14.41	−0.12/+0.12	13.63	−0.12/+0.12	13.45	−0.12/+0.12
SDSS J102109−0304	T3	I	14.11	−0.68/+0.52	13.43	−0.68/+0.52	13.33	−0.68/+0.52
SDSS J175033+1759.............	T3.5	I	14.13	−0.31/+0.27	13.73	−0.32/+0.28	13.30	−0.35/+0.32
SDSS J020742+0000.............	T4.5	I	14.47	−0.72/+0.54	14.59	−0.72/+0.54	14.23	−0.72/+0.54
2MASS J055919−1404.........	T5	I+O	13.78	−0.03/+0.03	13.63	−0.04/+0.04	13.53	−0.05/+0.06
2MASS J024313−2453.........	T6	I	15.27	−0.10/+0.09	15.00	−0.14/+0.14	15.10	−0.19/+0.19
2MASS J093734+2931..........	T6p	I	15.71	−0.11/+0.11	15.77	−0.07/+0.06	16.46	−0.14/+0.14
2MASS J122554−2739A......	T6:	I	14.92	−0.14/+0.14	14.92	−0.16/+0.16	14.73	−0.20/+0.20
SDSS J134646−0031	T6	I	15.09	−0.16/+0.15	15.16	−0.17/+0.16	15.09	−0.24/+0.23
SDSS J162414+0029.............	T6	I+O	15.13	−0.06/+0.05	15.21	−0.07/+0.06	15.31	−0.13/+0.13
2MASS J235654−1553.........	T6	I	15.05	−0.12/+0.12	14.83	−0.15/+0.15	14.99	−0.21/+0.21
2MASS J104753+2124..........	T6.5	I	15.71	−0.13/+0.13	15.72	−0.13/+0.13	15.98	−0.13/+0.13
2MASS J123739+6526.........	T6.5e	I	15.88	−0.13/+0.13	15.83	−0.15/+0.15	16.06	−0.23/+0.23
2MASS J072718+1710.........	T7	I	15.84	−0.08/+0.08	15.94	−0.18/+0.18	15.79	−0.20/+0.20
2MASS J121711−0311	T7.5	I	16.09	−0.13/+0.13	15.95	−0.17/+0.17	15.91	−0.17/+0.17
2MASS J122554−2739B	T8:	I	16.27	−0.14/+0.14	16.27	−0.16/+0.16	16.08	−0.20/+0.20
2MASS J041519−0935.........	T8/T9	I	16.92	−0.07/+0.07	16.73	−0.12/+0.11	16.66	−0.20/+0.20

applicable to the primary for determining M_H and M_K is reasonable.

For 2MASS J114634+2230AB, Reid et al. (2001) estimate a J-band magnitude difference of $\Delta M = 0.23$, again based on optical colors from *HST* WFPC2 observations, and we again use this magnitude difference to correct the J magnitude for

the L3 primary component and assume that the combined light JHK colors apply to the primary. The small difference in ΔM indicates that the B component must be near an L3 also and that our assumption that the system JHK colors are applicable to the primary for determining M_H and M_K is reasonable.

TABLE 8
DERIVED L AND T DWARF BOLOMETRIC MAGNITUDES, LUMINOSITIES, AND $T_{\rm eff}$

Star (1)	Spectral Type (2)	$M_{\rm bol} \pm \sigma({\rm M_{bol}})$ (3)	$\log (L/L_\odot) \pm \sigma[\log (L/L_\odot)]$ (4)	$T_{\rm eff} \pm \sigma\,(T_{\rm eff})$ (K) (5)
2MASS J034543+2540.........	L0	13.68 ± 0.14	-3.58 ± 0.06	2426^{+246}_{-191}
SDSS J143517−0046............	L0	13.53 ± 1.29	-3.52 ± 0.52	2511^{+915}_{-664}
SDSS J225529−0034............	L0:	13.59 ± 0.39	-3.54 ± 0.16	2477^{+338}_{-276}
2MASS J074642+2000A.......	L0.5	13.84 ± 0.14	-3.64 ± 0.06	2338^{+238}_{-187}
2MASS J143928+1929.........	L1	13.98 ± 0.14	-3.70 ± 0.06	2264^{+230}_{-181}
2MASS J165803+7027..........	L1	13.87 ± 0.14	-3.65 ± 0.06	2322^{+236}_{-186}
Kelu−1.................................	L2	13.76 ± 0.16	-3.61 ± 0.06	2382^{+246}_{-195}
DENIS J1058.7−1548..........	L3	14.79 ± 0.14	-4.02 ± 0.06	1879^{+191}_{-150}
2MASS J114634+2230A.......	L3	14.39 ± 0.14	-3.86 ± 0.06	2060^{+209}_{-165}
2MASS J143535−0043.........	L3	14.41 ± 0.84	-3.87 ± 0.34	2051^{+489}_{-386}
2MASS J003616+1821.........	L3.5	14.69 ± 0.13	-3.98 ± 0.05	1923^{+193}_{-153}
2MASS J032613+2950.........	L3.5	14.56 ± 0.18	-3.93 ± 0.07	1981^{+209}_{-166}
2MASS J184108+3117.........	L4 pec	14.45 ± 0.23	-3.88 ± 0.09	2032^{+226}_{-181}
2MASS J222443−0158.........	L4.5	15.09 ± 0.14	-4.14 ± 0.06	1753^{+179}_{-140}
SDSS J053952−0059............	L5	15.25 ± 0.15	-4.20 ± 0.06	1690^{+173}_{-137}
DENIS J122815−1547A	L5	15.30 ± 0.16	-4.22 ± 0.06	1671^{+172}_{-137}
DENIS J122815−1547B	L5	15.30 ± 0.16	-4.22 ± 0.06	1671^{+172}_{-137}
2MASS J132855+2114.........	L5	14.93 ± 0.30	-4.08 ± 0.12	1819^{+221}_{-178}
SDSS J144600+0024.............	L5	15.51 ± 0.22	-4.31 ± 0.09	1592^{+175}_{-140}
2MASS J150747−1627.........	L5	15.41 ± 0.13	-4.27 ± 0.05	1629^{+164}_{-129}
SDSS J010752+0041.............	L5.5	16.04 ± 0.21	-4.52 ± 0.08	1409^{+153}_{-122}
2MASS J085035+1057A........	L6	15.81 ± 0.43	-4.43 ± 0.17	1486^{+214}_{-175}
2MASS J095105+3558..........	L6	14.47 ± 1.10	-3.89 ± 0.44	2023^{+624}_{-471}
2MASS J171145+2232..........	L6.5	15.64 ± 0.36	-4.36 ± 0.14	1545^{+203}_{-165}
2MASS J003030−1450.........	L7	15.64 ± 0.31	-4.36 ± 0.12	1545^{+190}_{-154}
2MASS J172811+3948A.......	L7	16.04 ± 0.22	-4.52 ± 0.09	1409^{+155}_{-124}
DENIS J020529−1159A	L7	15.59 ± 0.15	-4.34 ± 0.06	1563^{+160}_{-127}
DENIS J020529−1159B	L7	15.59 ± 0.15	-4.34 ± 0.06	1563^{+160}_{-127}
SDSS J042348−0414............	L7.5/T0	15.28 ± 0.16	-4.22 ± 0.06	1678^{+174}_{-137}
2MASS J082519+2115..........	L7.5	16.12 ± 0.15	-4.55 ± 0.06	1383^{+142}_{-112}
2MASS J210115+1756A.......	L7.5	16.30 ± 0.31	-4.62 ± 0.12	1327^{+163}_{-132}
SDSS J003259+1410.............	L8	15.58 ± 0.41	-4.34 ± 0.16	1566^{+220}_{-179}
2MASS J032842+2302.........	L8	15.67 ± 0.31	-4.37 ± 0.12	1534^{+189}_{-153}
SDSS J083008+4828.............	L8	16.30 ± 0.18	-4.62 ± 0.07	1327^{+140}_{-111}
SDSS J132629−0038............	L8?	15.84 ± 0.32	-4.44 ± 0.13	1475^{+184}_{-149}
2MASS J152322+3014.........	L8	16.29 ± 0.19	-4.62 ± 0.08	1330^{+142}_{-112}
2MASS J163229+1904.........	L8	16.24 ± 0.16	-4.60 ± 0.06	1346^{+139}_{-110}
SDSS J083717−0000............	T0.5	16.59 ± 0.93	-4.74 ± 0.37	1241^{+326}_{-252}
SDSS J015141+1244..............	T1 $\pm$ 1	16.43 ± 0.31	-4.68 ± 0.12	1288^{+158}_{-128}
SDSS J125453−0122.............	T2	16.19 ± 0.19	-4.58 ± 0.08	1361^{+145}_{-115}
SDSS J102109−0304.............	T3	15.93 ± 0.62	-4.48 ± 0.25	1445^{+267}_{-216}
SDSS J175033+1759.............	T3.5	15.83 ± 0.37	-4.44 ± 0.15	1478^{+197}_{-160}
SDSS J020742+0000.............	T4.5	16.63 ± 0.65	-4.76 ± 0.26	1230^{+236}_{-191}
2MASS J055919−1404.........	T5	15.86 ± 0.17	-4.45 ± 0.06	1469^{+153}_{-122}
2MASS J024313−2453.........	T6	17.31 ± 0.25	-5.03 ± 0.10	1052^{+119}_{-97}
2MASS J093734+2931..........	T6p	18.67 ± 0.21	-5.57 ± 0.08	769^{+85}_{-69}
2MASS J122554−2739A......	T6:	16.94 ± 0.27	-4.88 ± 0.11	1145^{+133}_{-188}
SDSS J134646−0031............	T6	17.30 ± 0.29	-5.02 ± 0.12	1054^{+126}_{-102}
SDSS J162414+0029.............	T6	17.52 ± 0.20	-5.11 ± 0.08	1002^{+98}_{-86}
2MASS J235654−1553.........	T6	17.20 ± 0.26	-4.98 ± 0.10	1079^{+124}_{-100}
2MASS J104753+2124..........	T6.5	18.14 ± 0.20	-5.36 ± 0.08	869^{+93}_{-75}
2MASS J123739+6526.........	T6.5e	18.22 ± 0.28	-5.39 ± 0.11	853^{+101}_{-82}
2MASS J072718+1710..........	T7	17.90 ± 0.25	-5.26 ± 0.10	918^{+105}_{-84}
2MASS J121711−0311	T7.5	17.98 ± 0.23	-5.30 ± 0.09	901^{+101}_{-80}
2MASS J122554−2739B	T8:	18.12 ± 0.27	-5.35 ± 0.11	873^{+102}_{-82}
2MASS J041519−0935.........	T8/T9	18.70 ± 0.26	-5.58 ± 0.10	764^{+88}_{-71}

TABLE 9
MEAN L AND T DWARF CHARACTERISTICS

Spectral Type	M_J	M_H	M_K	$J-H$	$J-K$	M_{bol}	$\log (L/L_\odot)$	T_{eff} (K)
L0	11.62	10.85	10.33	0.77	1.29	13.54	−3.52	2510
L0.5	11.81	11.02	10.49	0.79	1.32	13.73	−3.60	2400
L1	12.00	11.19	10.65	0.81	1.35	13.92	−3.67	2300
L1.5	12.19	11.36	10.81	0.83	1.38	14.10	−3.74	2200
L2	12.38	11.54	10.98	0.84	1.40	14.29	−3.82	2110
L2.5	12.57	11.71	11.14	0.86	1.43	14.46	−3.89	2030
L3	12.76	11.88	11.30	0.88	1.46	14.63	−3.96	1950
L3.5	12.95	12.05	11.46	0.90	1.49	14.80	−4.02	1870
L4	13.14	12.22	11.62	0.92	1.52	14.97	−4.09	1800
L4.5	13.33	12.39	11.79	0.94	1.54	15.13	−4.16	1740
L5	13.52	12.57	11.95	0.95	1.57	15.29	−4.22	1670
L5.5	13.71	12.74	12.11	0.97	1.60	15.44	−4.28	1620
L6	13.90	12.91	12.27	0.99	1.63	15.58	−4.34	1570
L6.5	14.09	13.09	12.43	1.00	1.66	15.72	−4.39	1520
L7	14.28	13.26	12.59	1.02	1.69	15.85	−4.44	1470
L7.5	14.47	13.43	12.76	1.04	1.71	15.99	−4.50	1430
L8	14.66	13.60	12.92	1.06	1.74	16.11	−4.55	1390
T0.5	14.79	13.60	13.21	1.19	1.58	16.14	−4.56	1380
T1	14.60	13.58	13.23	1.02	1.37	16.10	−4.54	1390
T1.5	14.44	13.59	13.27	0.85	1.17	16.08	−4.54	1400
T2	14.33	13.63	13.35	0.70	0.98	16.09	−4.54	1390
T2.5	14.27	13.70	13.46	0.57	0.81	16.11	−4.55	1390
T3	14.26	13.80	13.60	0.46	0.66	16.20	−4.58	1360
T3.5	14.28	13.93	13.77	0.35	0.51	16.30	−4.62	1330
T4	14.36	14.10	13.96	0.26	0.40	16.42	−4.67	1290
T4.5	14.48	14.29	14.19	0.19	0.29	16.59	−4.74	1240
T5	14.64	14.52	14.45	0.12	0.19	16.78	−4.82	1190
T5.5	14.85	14.78	14.74	0.07	0.11	17.01	−4.91	1130
T6	15.11	15.07	15.06	0.04	0.05	17.27	−5.01	1060
T6.5	15.41	15.39	15.41	0.02	0.00	17.57	−5.13	990
T7	15.75	15.74	15.79	0.01	−0.04	17.90	−5.26	920
T7.5	16.14	16.12	16.20	0.02	−0.06	18.27	−5.41	840
T8	16.58	16.53	16.64	0.05	−0.06	18.68	−5.58	770

17. ABSOLUTE *JHK* MAGNITUDES BASED ON OPTICAL AND INFRARED PARALLAXES

In this section, we combine the adopted spectral types and CIT system photometry from Table 6 with the infrared parallaxes presented in this paper (Table 2) and the optical parallaxes derived by D02 to derive CIT system absolute magnitudes M_J, M_H, and M_K. These are presented in Table 7 in order of spectral type. We note that the spectral types used for the objects in D02 conform to the convention for L and T spectral types described in § 13. In the seven cases where both USNO optical and infrared parallaxes are available, we combined the parallaxes, weighting by the listed uncertainties. The first three columns give the abbreviated object names, adopted spectral type, and whether optical, infrared, or combined parallaxes were used, respectively. The last six columns give M_J, M_H, and M_K, and their uncertainties, respectively. We have not included the B components of binaries where spectral types are uncertain.

For the 36 objects from L0 to L8 (excluding the enigmatic object SDSS J042348−0414), we use the data of Table 7 to derive the following equations giving the best linear fits of M_J, M_H, and M_K, respectively, with spectral type (ST), where we numerically encode $\mathrm{ST}_L = 0$ for L0, $\mathrm{ST}_L = 5$ for L5, etc. There is no evidence for significant second-order terms for any of the bandpasses. We weighted the data by the inverse square of the larger of the $\sigma(-/+)$ values and, since these are all "preliminary" parallaxes degraded the minimum error to

0.05 mag such that the few objects with very small formal errors would not dominate the fits. The uncertainties listed at the end of each equation show the dispersions from the fits, in magnitudes:

$$M_J = 11.62 + 0.380(\mathrm{ST}_L), \quad \sigma = 0.24, \quad (1)$$

$$M_H = 10.85 + 0.346(\mathrm{ST}_L), \quad \sigma = 0.19, \quad (2)$$

$$M_K = 10.33 + 0.324(\mathrm{ST}_L), \quad \sigma = 0.17. \quad (3)$$

The changing slopes with bandpass reflect the fact that the L dwarfs become redder with later spectral type. Our results are consistent with those of D02 who report an M_J slope of 0.347 and scatter of $\sigma = 0.24$ mag for objects between M6.5 V and L8.

For the 19 T dwarfs between T0.5 and T8, the following quadratic equations adequately describe the M_J, M_H, and M_K versus spectral relations where $\mathrm{ST}_T = 0$ for T0, $\mathrm{ST}_T = 5$ for T5, etc. In this case, we have degraded the minimum uncertainty to 0.10 mag so that essentially one object would not dominate the fit:

$$M_J = 15.04 - 0.533(\mathrm{ST}_T) + 0.091(\mathrm{ST}_T)^2, \quad \sigma = 0.36, \quad (4)$$

$$M_H = 13.66 - 0.139(\mathrm{ST}_T) + 0.063(\mathrm{ST}_T)^2, \quad \sigma = 0.44, \quad (5)$$

$$M_K = 13.22 - 0.055(\mathrm{ST}_T) + 0.060(\mathrm{ST}_T)^2, \quad \sigma = 0.62. \quad (6)$$

18. L AND T DWARF LUMINOSITIES AND EFFECTIVE TEMPERATURE ESTIMATES

L and T dwarf luminosities and effective temperatures can be estimated for objects with known distances. D02 have previously made such estimates for mid M stars through late L dwarfs, but this has been difficult to do for T dwarfs due to the paucity of bolometric corrections ($BC_{filt} = M_{bol} - M_{filt}$) that have previously been measured for these objects (e.g., for 2MASS J055919$-$1404, Burgasser 2001; for Gl 229B, Leggett et al. 1999, Leggett et al. 2002; for Gl 570D, Burgasser et al. 2000, Geballe et al. 2001, Leggett et al. 2002). However, Golimowski et al. (2004) have recently calculated BC_K for a large number of both L and T dwarfs, greatly expanding the number of consistently derived bolometric corrections available for these objects. Moreover, they have included L' and M' photometry in their BC calculations, such that most of the spectral energy distributions of L and T dwarfs are now covered for the first time, allowing more reliable estimates of bolometric corrections and, hence, bolometric magnitudes to be made.

We use the M_K values from Table 7 and apply the fourth-order polynomial fit of BC_K versus spectral type from Table 4 of Golimowski et al. (2004) to determine M_{bol} for L and T dwarfs that have USNO parallaxes. The resultant M_{bol} values, along with their balanced uncertainties, are listed in column (3) of Table 8. We note that the M_K values are on the CIT system, while the Golimowski et al. (2004) BC_K determinations are formally for the K_{MKO} filter. However, the synthetic transformations of Stephens & Leggett (2004) show that the CIT and MKO filters give nearly identical results for L and T dwarfs with offsets of 0.01–0.02 mag for L0–L8 and 0.02–0.09 mag for T0.5–T8. These small offsets are dominated by other sources of uncertainty but are added to the error budget. In addition, the Golimowski et al. (2004) BC_K versus spectral type calibration is for the spectral classification system of Geballe et al. (2002), which includes L and T spectral types as late as L9 and T9, but we expect no significant effects from this. The errors listed for M_{bol} are the quadrature sums of the following uncertainties: $0.02 \leq \sigma(M_K) \leq 1.28$ mag, $0.01 \leq \sigma(K_{CIT} - K_{MKO}) \leq 0.09$ mag, and $\sigma(BC) = 0.13$ mag. Assuming for the Sun $M_{bol} = +4.74$ (Drilling & Landolt 2000), we list the derived logarithmic luminosities in units of solar luminosity along with their uncertainties in column (4) of Table 8.

Effective temperatures (T_{eff}) for L and T dwarfs can be estimated from $L = 4\pi R^2 \sigma T_{eff}^4$, normalized to solar units, by

$$M_{bol} = 42.36 - 5 \log (R/R_\odot) - 10 \log T_{eff} \qquad (7)$$

(Drilling & Landolt 2000). L and T dwarf radii are largely, but not totally, independent of mass and age, with a range of about 30%. Burgasser (2001) performed a Monte Carlo analysis of the Burrows et al. (1997) L and T dwarf evolutionary models, to understand the distribution of radii for objects between 0.001 and 10 Gyr in age and masses between 1.0 and 100 M_J. The mean radius for the model assuming constant birth rate and the mass function $dN \propto M^{-1}dM$ is 0.90 R_J. A total radius range of about 0.75–1.05 R_J results from these simulations. We use a radius of 0.90 ± 0.15 R_J and the previously derived values of M_{bol} and its uncertainties to derive the T_{eff} values and their range, which are listed in the last column of Table 8. At $\log (L/L_\odot) = -5.58 \pm 0.10$ and $T_{eff} \approx 760$ K, 2MASS J041519$-$0935 is found to be the coldest and least luminous brown dwarf yet discovered.

While luminosities and temperatures drop quickly with spectral type for early L and late T objects, the derived values of M_{bol} and $\log (L/L_\odot)$ show only a small range between about L6–T5. When combined with the assumptions about brown dwarf radii above, this implies a temperature range of only about 1200–1550 K. A similar narrow range in T_{eff} was predicted by Kirkpatrick et al. (2000) based on luminosity estimates for Gl 584C (L8) and Gl 229B (T6.5). Such a narrow T_{eff} range over a substantial shift in spectral morphology is predicted by Burgasser et al. (2002b), who postulate that the L–T transition is dominated by condensate cloud evolution, rather than cooling. However, more recent cloud models (e.g., Tsuji & Nakajima 2003) also predict a rapid evolution from L to T without the need for atmospheric dynamics. Clearly, synoptic monitoring, over a range of timescales, both photometrically and spectroscopically, will need to be a high priority in order to better understand the competition between cloud condensation and turbulent cloud disruption in these objects.

We note that our derived temperatures for the earliest L dwarfs of about 2400–2500 K are warmer by about 200–300 K than some earlier estimates (e.g., Leggett et al. 2001, 2002) but consistent with those derived by D02. We again direct attention to Golimowski et al. (2004), not only for their definitive BC calculations, but also for determinations of luminosities and temperatures for a somewhat different sample of objects, using a different photometric database and slightly different assumptions about brown dwarf radii.

19. MEAN DERIVED PROPERTIES OF L AND T DWARFS

In Table 9, we present mean derived properties of brown dwarfs based on the work of this paper. The spectral type ranges listed in column (1) (L0–L8 and T0.5–T8) span those of objects with USNO optical or infrared parallaxes. M_J, M_H, and M_K listed in columns (2), (3), and (4), respectively, are calculated from equations (1)–(6) of § 17, while the $J-H$ and $J-K$ colors in columns (5) and (6), respectively, are differences from these equations. M_{bol}, $\log (L/L_\odot)$, and T_{eff} in columns (7), (8), and (9), respectively, are derived from the listed M_K values and the methods discussed in § 18. T_{eff} values are rounded to the nearest 10 K. We caution that the values in Table 9 should be treated as schematic results only, since they do not represent the full width and subtle variations in the spectral type versus absolute magnitude relations of Figures 2–4. With better astrometry, photometry, and knowledge of brown dwarf variability, some of the apparent details in these figures may prove to be false, while others may prove to represent stellar and substellar physics.

20. FUTURE WORK

As with the USNO optical parallax and proper-motion program, it is our intent that the infrared astrometry program will be a long-term enterprise. All of the objects listed in this paper will be observed for a minimum of 3 yr to ensure a full distribution of observations over the parallactic ellipse, before final astrometric results are reported. Fainter objects and/or those with poorer reference frames will need a longer period of time. Our goal will be to provide 1.0 mas or better parallaxes for as many objects as possible, although it may not be a feasible goal for all objects. Objects with special astrophysical significance may be left on the program longer to achieve even higher precision.

It can be anticipated that many more brown dwarfs will be found by further mining of large-sky databases. Since objects

are removed from the current program as they are completed, new objects will be added to the program when they can fit into a depleted right ascension slot. We have already expanded our program from the initial 40 objects to 52 objects. Most of the new objects are T dwarfs, since we wish to use our resources on objects that are observed to advantage in the infrared while problematic for the optical CCD program. From experience with our current observing mode, a program consisting of 50–60 objects is a practical limit. We intend to publish an update to our results about every 2 yr, providing lists both of completed astrometry and preliminary results for new objects and objects with continuing observations.

A comparison of uncertainties listed in Tables 6 and 7 shows that for several objects the uncertainty in absolute magnitude is largely due to uncertainty in infrared photometry. We intend to provide high-quality USNO-CIT photometry, as in D02, for all objects for which we publish completed astrometry. These frames, along with the potential to obtain SDSS optical photometry from Flagstaff, will assure that photometric parallaxes of all suitable reference-frame stars will be available to form the best possible relative to absolute parallax corrections.

An interesting related issue is the question of how much of the spread in brown dwarf loci in the spectral type and color versus magnitude diagrams is due, not to mean intrinsic brightness dispersion, but to variability, especially for the L–T transition objects. The results of a several night photometric monitoring campaign during 1 month (Enoch et al. 2003) show variability for nine L and T dwarfs of 5%–25% in K_s band. Our astrometric database should prove to be valuable for investigation of J-band variability of T dwarfs and H-band variability of L dwarfs on timescales of minutes (one night's data), days (1 run's data), months (1 yr's data), and years (an entire astrometry data set).

21. SUMMARY

In this paper, we have presented preliminary parallaxes and proper motions for 22 L dwarfs and 18 T dwarfs derived over time baselines of only $\Delta t \approx 1.3$ or $\Delta t \approx 2.0$ yr. The resultant mean parallax uncertainties of 4.86 and 3.85 mas, respectively, which will be greatly improved by ongoing further observations, are nonetheless of sufficient quality to provide some significant new results for T dwarfs. We list here a summary of the more important conclusions we reach from our work.

1. The luminosity excess "hump" for early to mid T dwarfs in the absolute magnitude versus spectral type diagram is clearly confirmed. While seen most strongly at J band, it is also evident in the H and K bands. The possibility that the hump is due to a selection effect of binaries is likely ruled out by the large number of objects participating in the hump.

2. L5–L8 dwarfs have a significantly larger spread in the absolute magnitude versus spectral type diagrams than do earlier L dwarfs.

3. Late T dwarfs have a narrow locus in absolute magnitude versus spectral type diagrams, similar to the early L dwarfs. Relative to a straight line connecting the earlier and later

objects, the L–T transition objects show systematic trends. In J band the late L dwarfs show a luminosity deficit and the early T dwarfs a luminosity excess. The late L dwarf luminosity deficit is less in H band and is gone in K band, while the early T dwarf luminosity excess amplitude is somewhat less in H band and K band than at J band.

4. The absolute magnitude behavior across the L–T transition described above exemplifies the critical role of condensate cloud evolution at these temperatures based on the most recent spectral models.

5. Using newly derived bolometric corrections for L and T dwarfs by Golimowski et al. (2004), we derive luminosities and $T_{\rm eff}$ for L and T dwarfs with USNO-derived parallaxes either from this paper or D02.

6. 2MASS J041519−0935 is found to be the least luminous [$\log (L/L_\odot) = -5.58$] and therefore coldest ($T_{\rm eff} \approx 760$ K) brown dwarf yet found.

7. We find a broader distribution of L dwarf tangential velocities compared with that of the T dwarfs. While essentially the same between 20 and 60 km s^{-1}, the T dwarfs do not have a low-velocity population as do the L dwarfs. This is consistent with T dwarfs being, in general, older than L dwarfs.

REFERENCES

Abazajian, K., et al. 2003, AJ, 126, 2081
Basri, G. 2000, ARA&A, 38, 485
Becklin, E. E., & Zuckerman, B. 1988, Nature, 336, 656
Bessell, M. S., & Brett, J. M. 1988, PASP, 100, 1134
Burgasser, A. J. 2001, Ph.D. thesis, Caltech

Burgasser, A. J., et al. 2002a, ApJ, 564, 421
———. 1999, ApJ, 522, L65
———. 2000, ApJ, 531, L57
Burgasser, A. J., Kirkpatrick, J. D., Liebert, J., & Burrows, A. 2003b, ApJ, 594, 510

Burgasser, A. J., Kirkpatrick, J. D., Reid, I. N., Brown, M. E., Miskey, C. L., & Gizis, J. E. 2003a, ApJ, 586, 512

Burgasser, A. J., Marley, M. S., Ackerman, A. S., Saumon, D., Lodders, K., Dahn, C. C., Harris, H. C., & Kirkpatrick, J. D. 2002b, ApJ, 571, L151

Burrows, A., et al. 1997, ApJ, 491, 856

Carpenter, J. M. 2001, AJ, 121, 2851

Chabrier, G., & Baraffe, I. 2000, ARA&A, 38, 337

Cruz, K. L., Reid, I. N., Liebert, J., Kirkpatrick, J. D., & Lowrance, P. J. 2003, AJ, 126, 2421

Dahn, C. C. 1997, in IAU Symp. No. 189, Fundamental Stellar Properties: The Interaction Between Observation and Theory, ed. T. R. Bedding, A. J. Booth, & J. Davis (Dordrecht: Kluwer), 19

Dahn, C. C., et al. 2002, AJ, 124, 1170 (D02)

Delfosse, X., et al. 1997, A&A, 327, L25

Drilling, J. S., & Landolt, A. U. 2000, in Allen's Astrophysical Quantities, ed. A. Cox (4th ed.; New York: Springer), 382

Elias, J. H., Frogel, J. A., Matthews, K., & Neugebauer, G. 1982, AJ, 87, 1029 (erratum 87, 1893)

Enoch, M. L., Brown, M. E., & Burgasser, A. J. 2003, AJ, 126, 1006

Epchtein, N. 1997, in The Impact of Large Scale Near-IR Surveys, ed. F. Garzon et al. (Dordrecht: Kluwer), 15

Fan, X., et al. 2000, AJ, 119, 928

Fischer, J., et al. 2003, Proc. SPIE, 4841, 564

Fowler, A. M., Gatley, I., McIntyre, P., Vrba, F. J., & Hoffman, A. 1996, Proc. SPIE, 2816, 150

Geballe, T. R., Saumon, D., Leggett, S. K., Knapp, G. R., Marley, M. S., & Lodders, K. 2001, ApJ, 556, 373

Geballe, T. R., et al. 2002, ApJ, 564, 466

Gizis, J. E., Reid, I. N., Knapp, G. R., Liebert, J., Kirkpatrick, J. D., Koerner, D. W., & Burgasser, A. J. 2003, AJ, 125, 3302

Golimowski, D. A., et al. 2004, AJ, in press

Guetter, H. H., Vrba, F. J., Henden, A. A., & Luginbuhl, C. B. 2003, AJ, 125, 3344

Hawarden, T. G., Leggett, S. K., Letawsky, M. B., Ballantyne, D. R., & Casali, M. M. 2001, MNRAS, 325, 563

Hawley, S. L., et al. 2002, AJ, 123, 3409

Kirkpatrick, J. D., et al. 1999, ApJ, 519, 802

———. 2000, AJ, 120, 447

———. 2004, in preparation

Knapp, G. R., et al. 2004, AJ, in press

Koerner, D. W., Kirkpatrick, J. D., McElwain, M. W., & Bonaventura, A. J. 1999, ApJ, 526, L25

Leggett, S. K., Allard, F., Geballe, T. R., Hauschildt, P. H., & Schweitzer, A. 2001, ApJ, 548, 908

Leggett, S. K., et al. 2000, ApJ, 536, L35

———. 2002, ApJ, 564, 452

Leggett, S. K., Toomey, D. W., Geballe, T. R., & Brown, R. H. 1999, ApJ, 517, L139

Luginbuhl, C. B., Henden, A. A., Vrba, F. J., & Guetter, H. H. 1998, Proc. SPIE, 3354, 240

Luyten, W. J. 1979, NLTT Catalog (Minneapolis: Univ. Minnesota)

Martín, E. L., Delfosse, X., Basri, G., Goldman, B., Forveille, T., & Zapatero-Osorio, M. R. 1999, AJ, 118, 2466

Monet, D. G. & Dahn, C. C. 1983, AJ, 88, 1489

Monet, D. G., Dahn, C. C., Vrba, F. J., Harris, H. C., Pier, J. R., Luginbuhl, C. B., & Ables, H. D. 1992, AJ, 103, 638

Nakajima, T., Oppenheimer, B. R., Kulkarni, S. R., Golimowski, D. A., Matthews, K., & Durrance, S. T. 1995, Nature, 378, 463

Oppenheimer, B. R., Kulkarni, S. R., Matthews, K., & Nakajima, T. 1995, Science, 270, 1478

Reid, I. N., Gizis, J. E., Kirkpatrick, J. D., & Koerner, D. W. 2001, AJ, 121, 489

Schlegel, D. J., Finkbeiner, D. P., & Davis, M. 1998, ApJ, 500, 525

Schmidt-Kaler, Th. 1982, Landolt-Borstein, New Series, Group VI, 2b (New York: Springer), 453

Schneider, D. P., et al. 2002, AJ, 123, 458

Siegel, M. H., Majewski, S. R., Reid, I. N., & Thompson, I. B. 2002, ApJ, 578, 151

Skrutskie, M. F. et al. 1997, in The Impact of Large-Scale Near-IR Sky Surveys, ed. F. Garzon et al. (Dordrecht: Kluwer), 25

Smith, J. A. 2002, AJ, 123, 2121

Stephens, D. C. 2003, in IAU Symp. 211, Brown Dwarfs, ed. E. Martín (San Francisco: ASP), 355

Stephens, D. C., & Leggett, S. K. 2004, PASP, 116, 9

Stone, R. C. 1997, AJ, 114, 2811

Strauss, M. A., et al. 1999, ApJ, 522, L61

Tinney, C. G., Burgasser, A. J., & Kirkpatrick, J. D. 2003, AJ, 126, 975 (TBK03)

Tsuji, T., & Nakajima, T. 2003, ApJ, 585, L151

Tsvetanov, Z. I., et al. 2000, ApJ, 531, L61

Vrba, F. J., Henden, A. A., Luginbuhl, C. B., Guetter, H. H., & Monet, D. G. 2000, BAAS, 32, 678

York, D. G., et al. 2000, AJ, 120, 1579